














TECH BRIEFS

NATIONAL AERONAUTICS AND SPACE ADMINISTRATION

-  **Technology Focus**
-  **Electronics/Computers**
-  **Software**
-  **Materials**
-  **Mechanics**
-  **Machinery/Automation**
-  **Manufacturing & Prototyping**
-  **Bio-Medical**
-  **Physical Sciences**
-  **Information Sciences**
-  **Books and Reports**

INTRODUCTION

Tech Briefs are short announcements of innovations originating from research and development activities of the National Aeronautics and Space Administration. They emphasize information considered likely to be transferable across industrial, regional, or disciplinary lines and are issued to encourage commercial application.

Availability of NASA Tech Briefs and TSPs

Requests for individual Tech Briefs or for Technical Support Packages (TSPs) announced herein should be addressed to

National Technology Transfer Center

Telephone No. (800) 678-6882 or via World Wide Web at www2.nttc.edu/leads/

Please reference the control numbers appearing at the end of each Tech Brief. Information on NASA's Innovative Partnerships Program (IPP), its documents, and services is also available at the same facility or on the World Wide Web at <http://ipp.nasa.gov>.

Innovative Partnerships Offices are located at NASA field centers to provide technology-transfer access to industrial users. Inquiries can be made by contacting NASA field centers and Mission Directorates listed below.

NASA Field Centers and Program Offices

Ames Research Center

Lisa L. Lockyer
(650) 604-1754
lisa.l.lockyer@nasa.gov

Dryden Flight Research Center

Gregory Poteat
(661) 276-3872
greg.poteat@dfrc.nasa.gov

Goddard Space Flight Center

Nona Cheeks
(301) 286-5810
Nona.K.Cheeks.1@nasa.gov

Jet Propulsion Laboratory

Ken Wolfenbarger
(818) 354-3821
james.k.wolfenbarger@jpl.nasa.gov

Johnson Space Center

Helen Lane
(713) 483-7165
helen.w.lane@nasa.gov

Kennedy Space Center

Jim Aliberti
(321) 867-6224
Jim.Aliberti-1@nasa.gov

Langley Research Center

Ray P. Turcotte
(757) 864-8881
r.p.turcotte@larc.nasa.gov

John H. Glenn Research Center at Lewis Field

Robert Lawrence
(216) 433-2921
robert.f.lawrence@nasa.gov

Marshall Space Flight Center

Vernotto McMillan
(256) 544-2615
vernotto.mcmillan@msfc.nasa.gov

Stennis Space Center

John Bailey
(228) 688-1660
john.w.bailey@nasa.gov

NASA Mission Directorates

At NASA Headquarters there are four Mission Directorates under which there are seven major program offices that develop and oversee technology projects of potential interest to industry:

Carl Ray

Small Business Innovation Research Program (SBIR) & Small Business Technology Transfer Program (STTR)
(202) 358-4652
carl.g.ray@nasa.gov

Frank Schowengerdt

Innovative Partnerships Program (Code TD)
(202) 358-2560
fschowen@hq.nasa.gov

John Mankins

Exploration Systems Research and Technology Division
(202) 358-4659
john.c.mankins@nasa.gov

Terry Hertz

Aeronautics and Space Mission Directorate
(202) 358-4636
thertz@mail.hq.nasa.gov

Glen Mucklow

Mission and Systems Management Division (SMD)
(202) 358-2235
gmucklow@mail.hq.nasa.gov

Granville Paules

Mission and Systems Management Division (SMD)
(202) 358-0706
gpaules@mtpe.hq.nasa.gov

Gene Trinh

Human Systems Research and Technology Division (ESMD)
(202) 358-1490
eugene.h.trinh@nasa.gov

John Rush

Space Communications Office (SOMD)
(202) 358-4819
john.j.rush@nasa.gov



TECH BRIEFS

NATIONAL AERONAUTICS AND SPACE ADMINISTRATION



5 Technology Focus: Electronics

- 5 T-Shaped Emitter Metal Structures for HBTs
- 6 Rigorous Estimation of SNR of a PSK Communication Link
- 7 Advanced Ka-Band Transceiver With Monopulse Tracking
- 8 EMI Filters for Low-Temperature Applications
- 9 Lightweight Electronic Camera for Research on Clouds
- 9 Pilot Weather Advisor System



11 Electronics/Computers

- 11 Waveguide Power-Amplifier Module for 80 to 150 GHz
- 11 Better Back Contacts for Solar Cells on Flexible Substrates
- 12 Tunable, Highly Stable Lasers for Coherent Lidar
- 13 Optical Profilometers Using Adaptive Signal Processing
- 14 Improved Photon-Emission-Microscope System



15 Software

- 15 Program Synthesizes UML Sequence Diagrams
- 15 Aspect-Oriented Subprogram Synthesizes UML Sequence Diagrams
- 15 Updated Computational Model of Cosmic Rays Near Earth
- 15 Software for Alignment of Segments of a Telescope Mirror
- 16 Simulation of Dropping of Cargo With Parachutes
- 16 DAVE-ML Utility Programs
- 16 Robust Control for the Mercury Laser Altimeter



17 Materials

- 17 Thermally Stable Piezoelectric and Pyroelectric Polymers

- 17 Combustion Synthesis of $\text{Ca}_3(\text{PO}_4)_2$ Net-Shape Surgical Implants



19 Mechanics

- 19 Stochastic Representation of Chaos Using Terminal Attractors
- 20 Two High-Temperature Foil Journal Bearings
- 21 Using Plates To Represent Fillets in Finite-Element Modeling



23 Manufacturing & Prototyping

- 23 Repairing Chipped Silicide Coatings on Refractory Metal Substrates
- 23 Simplified Fabrication of Helical Copper Antennas



25 Physical Sciences

- 25 Graded-Index "Whispering-Gallery" Optical Microresonators
- 25 Manufacture of Sparse-Spectrum Optical Microresonators
- 26 Exact Tuning of High-Q Optical Microresonators by Use of UV



29 Information Sciences

- 29 Automation for "Direct-to" Clearances in Air-Traffic Control



31 Books & Reports

- 31 Improved Traps for Removing Gases From Coolant Liquids
- 31 Lunar Constellation of Frozen Elliptical Inclined Orbits

This document was prepared under the sponsorship of the National Aeronautics and Space Administration. Neither the United States Government nor any person acting on behalf of the United States Government assumes any liability resulting from the use of the information contained in this document, or warrants that such use will be free from privately owned rights.



T-Shaped Emitter Metal Structures for HBTs

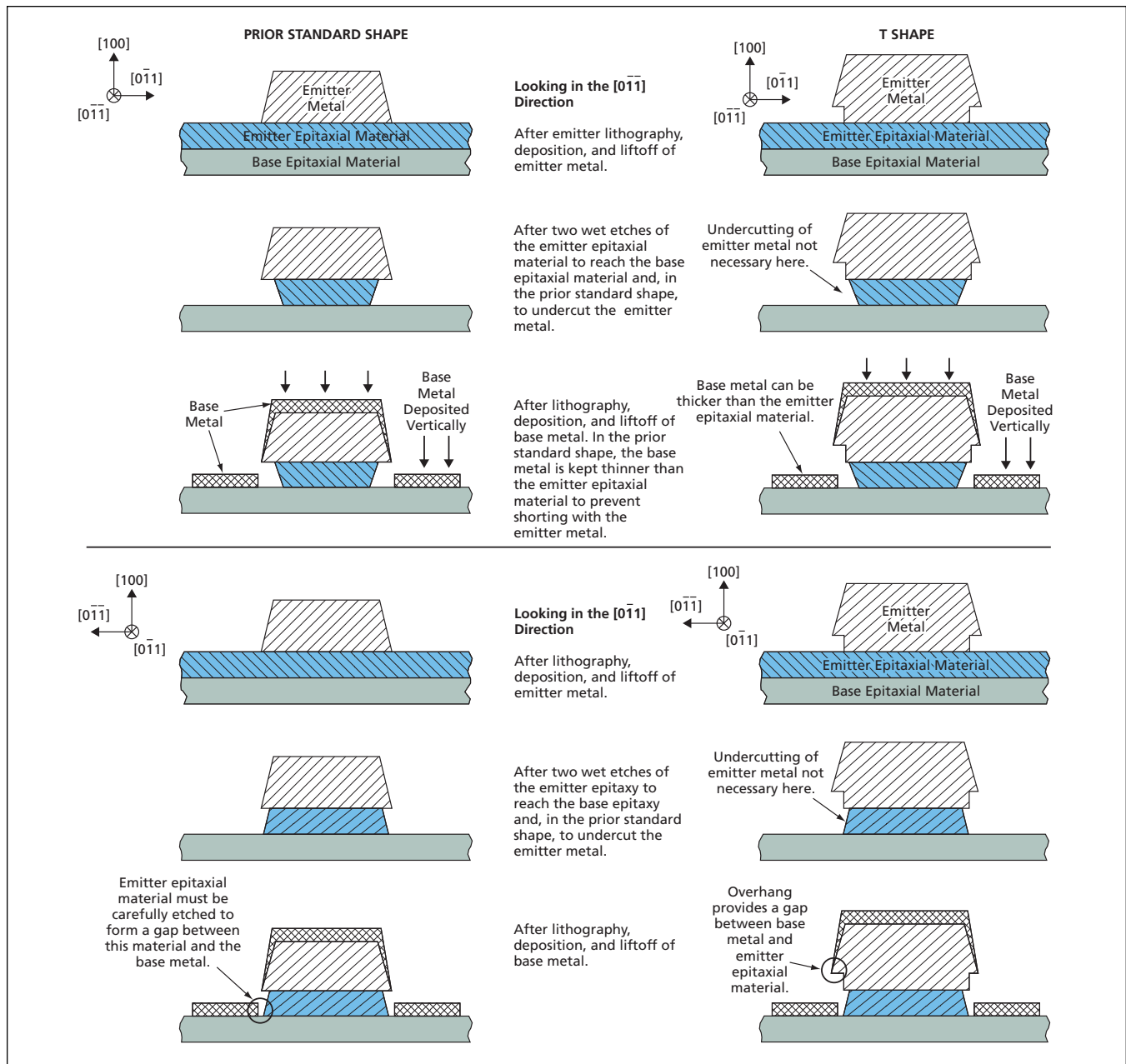
Fabrication yields are increased.

NASA's Jet Propulsion Laboratory, Pasadena, California

Metal emitter structures in a class of developmental InP-based high-speed heterojunction bipolar transistors (HBTs) have been redesigned to have T-shaped cross sections. More precisely,

the modified cross sections can be characterized as having highly stylized T shapes that are modified versions of prior trapezoidal shapes (see figure). T-cross-section metal features have been

widely used in Schottky diodes and high-electron-mobility transistors, but not in HBTs. As explained below, the purpose served by the present T cross-sectional shapes is to increase fabrication yields be-



Cross Sections of Base/Emitter Junctions containing self-aligned base metal structures, in the prior standard shape and the innovative T shape, are shown here at three stages of fabrication.

yond those achievable with the prior cross-sectional shapes.

At the beginning of the program to develop these HBTs, some of the HBTs were fabricated to contain self-aligned base metal structures and some to contain non-self-aligned base metal structures. For the ones containing self-aligned base metal structures, fabrication lots exhibited low yields and high degrees of nonuniformity, which were attributable to inadequate definition of base/emitter junctions. Yields were reduced by the need to reject transistors that had leaky junctions. One of the primary causes of leakage at the junctions was short-circuiting of the base metal to emitter semiconductor epitaxial material that had not been sufficiently removed from the vicinity of the base metal during the wet-etch undercut procedure. The existence of this cause was observed in some cases from scanning electron microscopy and indirectly deduced from the observation that the yields of HBTs containing non-

self-aligned base metal structures were more than double the yields of HBTs containing self-aligned base metal structures.

The incidence of leakage is smaller in the non-self-aligned case because the base metal is spaced farther from the emitter at the outset. In contrast, in the self-aligned case, the base metal is separated from the emitter epitaxial material by only the amount of the emitter undercut effected in the aforementioned etching. Self-aligned base metal structures are preferred over non-self-aligned ones because the resulting base resistances are smaller, leading to better transistor performances.

The T-shaped cross section reduces the likelihood of short-circuiting of base metal to epitaxial emitter material, thereby helping to increase fabrication yield, in the following way: The overhang portion of the T acts as an awning-like deposition mask. The base metal is deposited predominantly unidirectionally (vertically downward in the figure)

by evaporation, and deposition is prevented or reduced in the shadow area that lies under the overhang and adjacent to the emitter epitaxial material.

The T shape also offers other benefits:

- Requirements for controlling undercut etching are relaxed; as a consequence, emitter/base definition processes are simplified.
- The relaxation of requirements makes it possible to use thicker base metal deposits, thereby reducing the inductances and the electrical and thermal resistances of base metal structures.

This work was done by King Man Fung, Lorene Samoska, James Velebir, Richard Muller, Pierre Echternach, and Peter Siegel of Caltech; Peter Smith of Cree, Inc.; Suzanne Martin of Wavestream Corp.; Roger Malik of RfM Semiconductor; and Mark Rodwell, Miguel Urteaga, Vamsi Paidi, and Zack Griffith of UC Santa Barbara for NASA's Jet Propulsion Laboratory. Further information is contained in a TSP (see page 1). NPO-41034

Rigorous Estimation of SNR of a PSK Communication Link

It is not necessary to use a separate link to assess propagation conditions.

John H. Glenn Research Center, Cleveland, Ohio

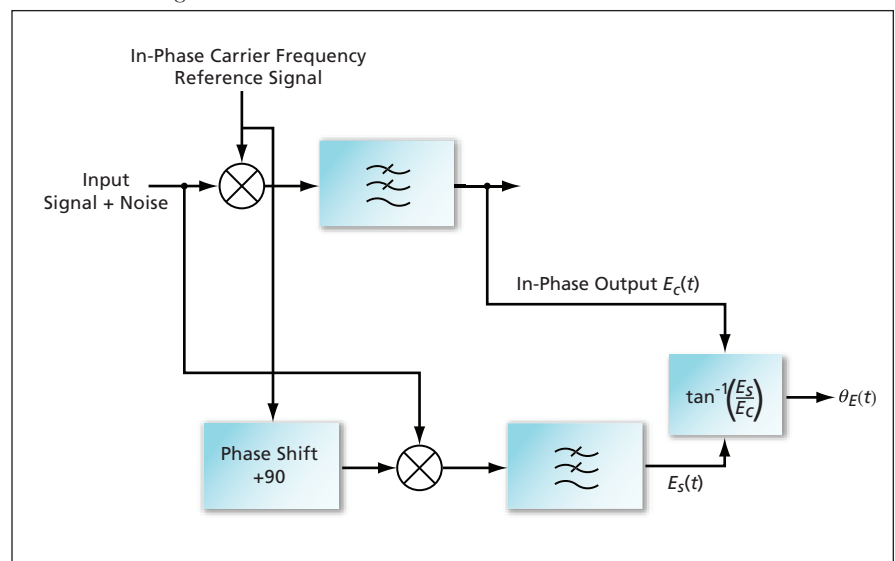
An improved method of estimating the signal-to-noise ratio (SNR) of a phase-shift keying (PSK) communication link is founded on a rigorous statistical analysis of the input to, and the output from, the PSK demodulator in the receiver. Many methods to estimate SNR ratios of PSK communication links have been developed previously, and all of them are defective (that is, not rigorous) in that all of them are based on tacit and unwarranted assumptions made for the sake of analytical simplification. In addition, some of the prior methods involve (1) the use of a separate receiver, denoted the propagation receiver, to measure a beacon signal distinct from the PSK communication signal and (2) extrapolation of the result of the measurement to an estimate the SNR of the PSK communication channel. In contrast, the improved method is free of unwarranted simplifying assumptions and does not require the use of a propagation receiver.

One basic concept shared by both the improved method and the prior methods is that the effect of noise in the communication link is not only present in the input to the demodulator but is also convolved within the

output of the demodulator. The mathematical analysis in this method is based on (1) established theories of statistical analysis of flows of the signal and noise through a generic M -ary PSK demodulator, and (2) techniques of maximum-likelihood estimation theory. In this analysis, one employs, rather than neglects, all the subtleties

of the statistics that characterize the stochastic nature of the phase-modulated signal to derive an estimation procedure that utilizes the inherent phase characteristics of the input to and the output from the demodulator.

The complexity of the analysis precludes a detailed description in this article. It must suffice to summarize as fol-



A PSK Demodulator Is Modified to obtain the phase error, $\theta_E(t)$, in a composite signal.

lows: The analysis begins with a description of the signal and noise in the case of binary PSK. This description serves as a foundation for a statistical connection between Gaussian noise and the SNR. This connection leads to a probabilistic description that establishes a rigorous connection between the SNR and the measured phase error of the BPSK signal entering the receiver demodulator. Then techniques of maximum-likelihood estimation theory are used to obtain analytical expressions for biased and unbiased estimates of the SNR from easily measured phase errors.

The method requires the use of a

modified BPSK demodulator to obtain the time-dependent phase error, $\theta_E(t)$ in a composite output signal. The SNR-estimation procedure begins with the acquisition of a sequence of samples $\theta_E(t_i)$ at k successive sampling times t_i ($i = 1$ to k). Next, one calculates a biased estimate, γ^* , of the SNR (γ) by use of the equation

$$\gamma^* = \kappa \left\{ \sum_{i=1}^k \sin^2 \theta_E(t_i) \right\}^{-1}$$

Finally, an unbiased estimate, $\hat{\gamma}$, is obtained from a lookup table that contains

solution values for a nonlinear equation that describes the relationship between γ^* and $\hat{\gamma}$. Although the method was derived for BPSK, it can be applied (with modifications) to quaternary and higher-order PSK.

This work was done by Robert M. Manning of Glenn Research Center. Further information is contained in a TSP (see page 1).

Inquiries concerning rights for the commercial use of this invention should be addressed to NASA Glenn Research Center, Commercial Technology Office, Attn: Steve Fedor, Mail Stop 4-8, 21000 Brookpark Road, Cleveland, Ohio 44135. Refer to LEW-17597-1.

Advanced Ka-Band Transceiver With Monopulse Tracking

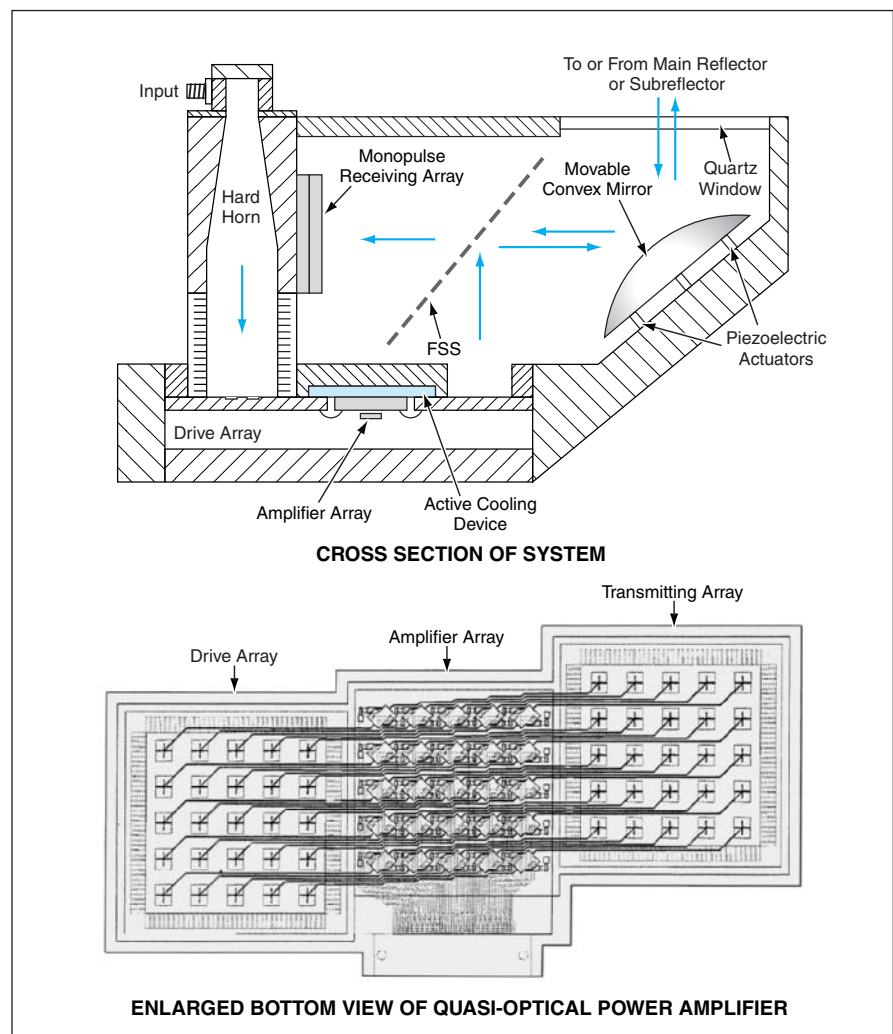
This system would offer advantages over a conventional TWTA-based system.

NASA's Jet Propulsion Laboratory, Pasadena, California

A proposed Ka-band transmitting/receiving system would embody a unique combination of established and semi-proven design features. Although this system is intended primarily for telecommunication use aboard a spacecraft, its design could be adapted to terrestrial military and commercial radar systems. Systems like this one could be especially suitable as replacements for prior systems in which traveling-wave-tube amplifiers (TWTAs) are used in the final transmitter stages.

The proposed system (see figure) would include a monopulse receiving feedback loop and a mirror that could be moved by piezoelectric actuators in the feedback loop to adjust the aim of the transmitted and received radio beams. Unlike in a phased-array tracking system, phase shifters (which can be complex and expensive) would not be needed in this monopulse tracking system. Moreover, the monopulse-tracking loop could be combined with other subsystems used in established subreflector and antenna designs.

Instead of a TWTA, the final transmitter power amplifier in the proposed system would be a quasi-optical power amplifier (QOPA) — a combination of a planar array of 25 amplifiers and corresponding planar arrays of antenna elements, such that free-space power combining would take place at the output. The goal of this QOPA would be to operate at a power of 20 W and produce a minimum gain



This Ka-Band Transmitting/Receiving System would include a monopulse tracking loop in the receiver and a quasi-optical power amplifier in the transmitter.

of 13 dB in the frequency range from 31.8 to 32.3 GHz.

The amplifiers would be identical to commercially available GaAs monolithic microwave integrated circuits (MMICs). Accompanying the QOPA, on the same circuit board, there would be two arrays of antenna elements: a drive array (a planar array of identical input antenna elements) and a transmitting array (a planar array of identical output antenna elements). The drive array would be fed via a hard horn, providing uniform illumination to each array element. By use of microstrip transmission lines, all of equal length, the input and output terminals of the MMIC amplifiers would be connected to the corresponding drive and transmitting antenna elements, respectively. This

QOPA design would offer the following advantages (among others):

- The separation of the input and output drive arrays helps eliminate the problem, encountered in prior QOPA systems, of oscillation and allows the use of high-gain amplifiers.
- Unlike a TWTA, the MMIC amplifiers would not necessitate a high-voltage power supply.
- The array of MMIC amplifiers could be actively cooled from its back side; unlike in prior QOPA arrays, it would not be necessary to rely on edge cooling, which is less effective and thus limits the achievable power to a lower level. This is important for future inclusion of wide band-gap devices such as GaN.
- The failure of a single amplifier would not be catastrophic: as long as the

other amplifiers continued to operate, the loss in performance would be relatively small. For maximum efficiency, the independent bias lines allow individual modules to be turned off as output power demands change.

The system would include a frequency-selective surface (essentially, a radio-frequency dichroic reflector) intended to reflect the transmitted beam while passing the received monopulse beam. The FSS would provide between 40 and 60 dB of isolation between the transmitted and received beams.

*This work was done by Abdur Khan, Dan Hoppe, Larry Epp, and Raul Perez of Caltech for NASA's Jet Propulsion Laboratory. Further information is contained in a TSP (see page 1).
NPO-30559*

EMI Filters for Low-Temperature Applications

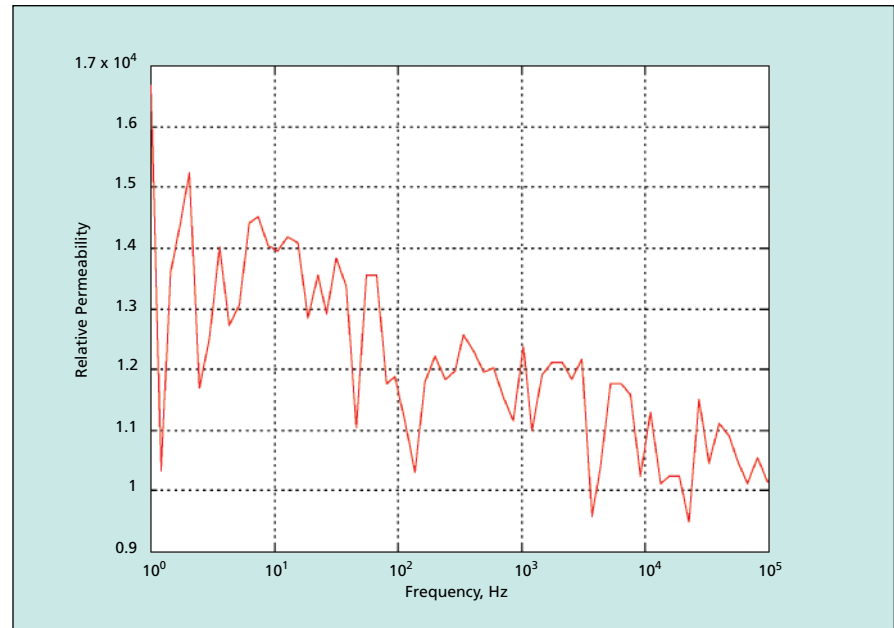
Unlike ferrite-core filters, these should work well under cryogenic conditions.

NASA's Jet Propulsion Laboratory, Pasadena, California

Filters that suppress electromagnetic interference (EMI) on signal cables connected to cryogenic electronic equipment can be made from cores consisting of high-permeability materials. The basic principle of operation of these filters is the same as that of the ferrite-core common-mode EMI filters now commonly used on cables that connect computers with peripheral equipment.

The ferrite-core filters are effective at room temperature but not at low temperatures, because their relative permeabilities decrease from $\approx 15,000$ at room temperature to ≈ 20 at a temperature of 4 K. In cases of cables that connect cryogenic electronic equipment with room-temperature electronic equipment, it has been common practice to place the ferrite filters at the room-temperature ends of the cables. This makes it necessary for the filtered signals to traverse the cables; during such traversal, crosstalk with other cables can cause the filtered signals to become recontaminated with EMI before they reach the cryogenic equipment. Hence, it would be preferable to place the EMI filters at the cryogenic ends of the cables. The present development makes this a viable option.

An inductive EMI filter blocks EMI due to its impedance to high frequency EMI signals. Since the impedance is proportional to the permeability, a material



Relative Permeability was measured with a superconducting quantum interference device (SQUID) magnetometer at 4 K.

with high permeability forms the core of such a filter. Several metallic alloys like Cryoperm 10 and VITROVAC are known to have relative permeability exceeding 14,000 at low temperature. However, their relative permeabilities decrease rapidly at frequencies higher than a few hundred hertz due to eddy current, which prevents the magnetic field from penetrating the material. Because ferrite is an

insulator, eddy current is not present. Therefore it works at high frequencies. However, all known materials with high permeabilities at low temperatures are metallic. Therefore, for the purpose of constructing cores for low-temperature EMI filters, it is desirable to prepare the high-permeability materials in the form of thin foils or fine powders to reduce the effects of eddy currents. Preliminary

measurements and calculations have shown that when foil thicknesses or particle sizes are reduced to <25 μm , eddy currents become unimportant.

We have performed low-temperature test (see figure) of a cobalt-based magnetic material made by Honeywell called Meglas 2714A, which has very

high permeability at room temperature and is available in form of tape-wound cores of various sizes. These cores are wound from 18- μm thick ribbons to reduce eddy current for high-frequency operations. The relative permeability is higher than 10,000 at frequencies up to 100 kHz, the limit of capability of our

measurement. EMI filters made from this material should work at low temperature.

This work was done by Talso Chui and Hung Quach of Caltech for NASA's Jet Propulsion Laboratory. Further information is contained in a TSP (see page 1). NPO-30901

Lightweight Electronic Camera for Research on Clouds

This camera would rapidly acquire image data on aerosol particles.

Goddard Space Flight Center, Greenbelt, Maryland

“Micro-CPI” (wherein “CPI” signifies “cloud-particle imager”) is the name of a small, lightweight electronic camera that has been proposed for use in research on clouds. The Micro-CPI would be incorporated into a small autonomous or remotely piloted airplane of a type that is now used in meteorological research and that is capable of remaining aloft for times long enough (typically about 30 hours) to collect statistically significant sets of data.

According to a preliminary design, the Micro-CPI would have a mass <1.5 kg and would consume less than 7 W of electric power. It would acquire and digitize high-resolution (3- μm -pixel) images of

ice particles and water drops at a rate up to 1,000 particles (and/or drops) per second. The Micro-CPI incorporates a particle detection laser that triggers the camera imaging laser, and also counts and sizes very small (<1- μm) aerosol particles and cloud drops up to about 100 μm in diameter. The Micro-CPI could record data for an observation time of more than 30 hours and could operate autonomously.

Although a quantitative estimate of the cost of the Micro-CPI is not yet available, it has been projected that the cost would be low, relative to the costs of cameras of conventional design that could offer the same imaging capabili-

ties. This is fortunate because there could be a potential need in the coming years to launch hundreds or even thousands of small uninhabited aircraft carrying cameras of Micro-CPI design as part of an effort to measure properties of clouds on a global scale. There are also potential applications in the measurement of drop-size distributions in sprays, especially in the agricultural and painting industries.

This work was done by Paul Lawson of SPEC Inc. for Goddard Space Flight Center. Further information is contained in a TSP (see page 1). GSC-14950-1

Pilot Weather Advisor System

Cockpit displays of weather affecting flight are updated every five minutes.

John H. Glenn Research Center, Cleveland, Ohio

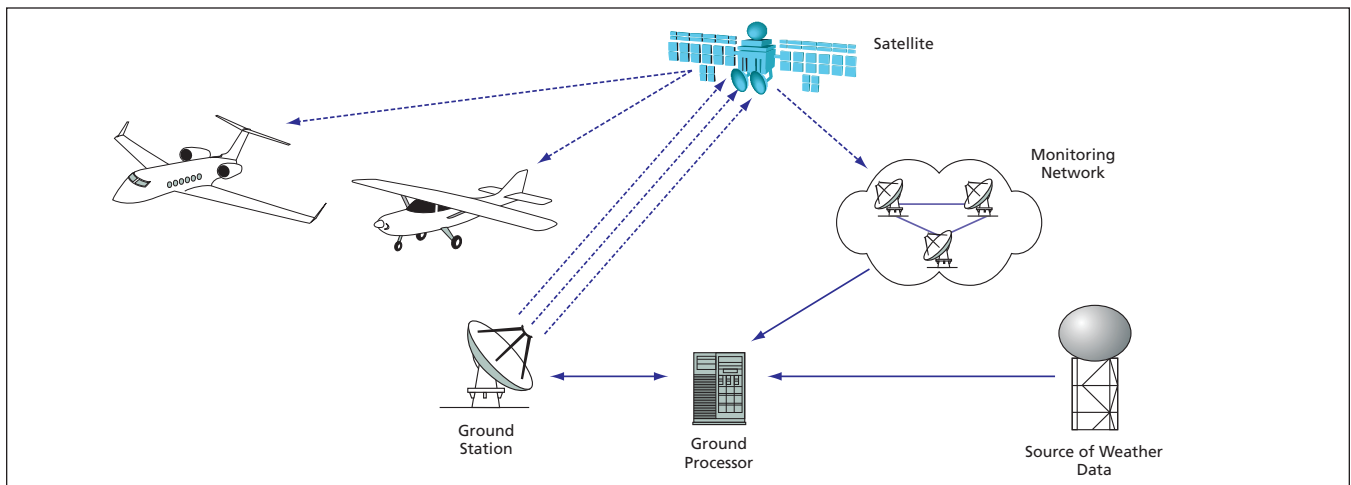
The Pilot Weather Advisor (PWA) system is an automated satellite radio-broadcasting system that provides nearly real-time weather data to pilots of aircraft in flight anywhere in the continental United States. The system was designed to enhance safety in two distinct ways: First, the automated receipt of information would relieve the pilot of the time-consuming and distracting task of obtaining weather information via voice communication with ground stations. Second, the presentation of the information would be centered around a map format, thereby making the spatial and temporal relationships in the surrounding weather situation much easier to understand. Starting in the early 1990s, the PWA system was developed by ViGYAN, Inc., under the NASA SBIR program. The system recently became

commercially viable and was sold to WSI, a leading provider of weather services in aviation. The system is now marketed under the brand name “WSI InFlight.”

The PWA system includes a ground processor (see figure), wherein a computer running special-purpose software converts, compresses, and schedules the weather data. The compressed data are then transmitted through a ground station to a geosynchronous satellite, from whence they are broadcast to cover the continental United States. The signal is acquired by a light, low-drag antenna mounted on a subscriber's aircraft, and is then interpreted by an equally lightweight receiver. In the cockpit of each InFlight equipped aircraft, the data are processed, by use of other special-purpose software and hardware, into an

easy-to-interpret graphical display. The display is presented on a portable or panel-mounted unit. The data, which include graphical meteorological aviation reports (METARs), terminal aerodrome forecasts (TAFs), and Next Generation Weather Radar (NEXRAD) images, as well as other weather products, are updated every five minutes.

Accessibility of the system to light general aviation was a design goal because such airplanes are more susceptible to changes in weather than are larger, higher-flying airplanes. The lightweight, low-drag nature of the PWA airborne components and the relatively low cost of acquiring and using the equipment make the PWA system affordable for incorporation into lower-cost single-engine airplanes, which constitute the largest segment of the aviation market. Hence,



The Pilot Weather Advisor System is designed to enhance the weather-related safety of general aviation aircraft by providing frequent weather updates.

success of this design goal was achieved. In addition, the PWA system is also attractive for use in higher-priced general-aviation airplanes because the weather information that it provides covers longer ranges than do onboard weather radar and lightning detectors with which such airplanes are often equipped.

This work was done by Glenn Lindamood and Konstantinos (Gus) Martzaklis of Glenn Research Center; Keith Hoffler, Damon Hill, Sudhir C. Mehrotra, and E. Richard White of ViGYAN, Inc.; Bruce D. Fisher of NASA Langley Research Center; Norman L. Crabill of Aero Space Consultants; and Allen D. Tucholski of Akima Corp.

Further information is contained in a TSP (see page 1).

Inquiries concerning rights for the commercial use of this invention should be addressed to NASA Glenn Research Center, Innovative Partnerships Office, Attn: Steve Fedor, Mail Stop 4-8, 21000 Brookpark Road, Cleveland, Ohio 44135. Refer to LEW-17702-1.



Waveguide Power-Amplifier Module for 80 to 150 GHz

The amplifier can now be connected to other equipment more easily.

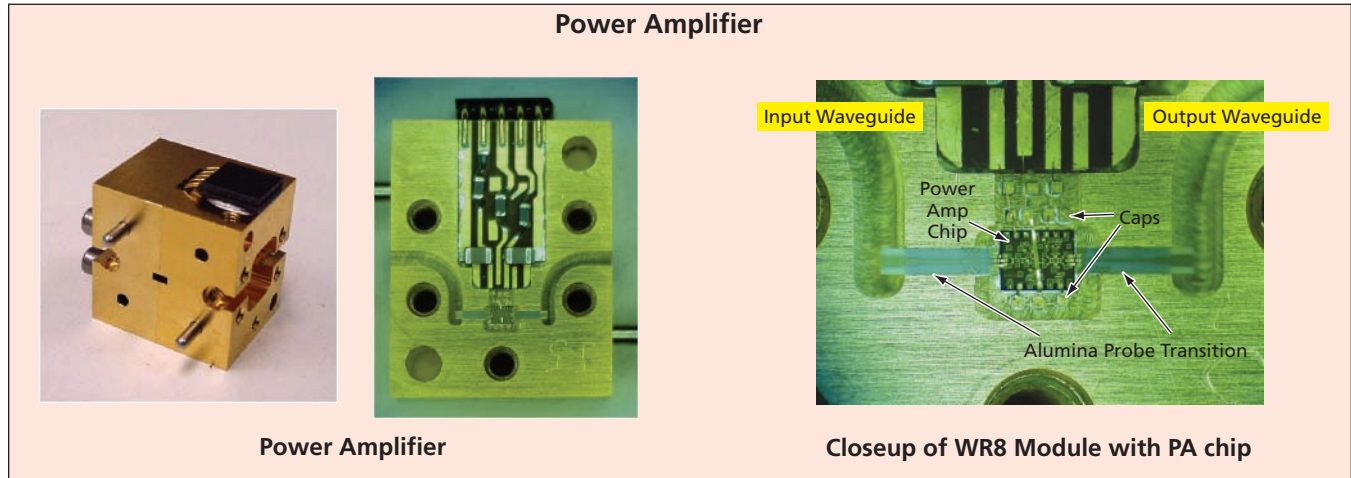
NASA's Jet Propulsion Laboratory, Pasadena, California

A waveguide power-amplifier module capable of operating over the frequency range from 80 to 150 GHz has been constructed. The module comprises a previously reported power amplifier packaged in a waveguide housing that is

amplifier must be connected for normal operation.

The amplifier in its unpackaged form was reported in "Power Amplifier With 9 to 13 dB of Gain from 65 to 146 GHz" (NPO-20880), *NASA Tech Briefs*, Vol. 25,

form. In addition to packaging in a waveguide housing, the amplifier was modified to suppress low-frequency oscillations, to which the amplifier was previously susceptible because it had high gain at DC. The modifications con-



The **Amplifier Module** features a housing that is compatible with WR-8 waveguides. (Note: The largest dimension of the waveguide block is smaller than the size of a quarter.)

compatible with WR-8 waveguides. (WR-8 is a standard waveguide size for the nominal frequency range from 90 to 140 GHz.) Because the amplifier in its unpackaged form was a single, fragile InP chip, it was necessary to use special probes to make electrical connections between the amplifier and test equipment in order to measure the power gain and other aspects of amplifier performance. In contrast, the waveguide power-amplifier module is robust and can be bolted to test equipment and to other electronic circuits with which the

No. 1 (January 2001), page 44. To recapitulate: the amplifier provides three stages of amplification, implemented by means of four InP high-electron-mobility transistors in a grounded coplanar waveguide circuit with lumped-element interstage and shunt capacitors. The circuit also features a unique coplanar waveguide power-combining structure in the output stage. The output radio-frequency power was measured to be 25 to 40 mW from 106 to 140 GHz.

The figure shows selected aspects of the amplifier in its present packaged

sisted mostly of special placement of bypass capacitors and radio-frequency chokes within the package. The packaged amplifier was found to operate stably, and to produce a gain of at least 7 dB while producing output power of at least 10 mW at frequencies from 80 to 150 GHz.

This work was done by Lorene Samoska, Sander Weinreb, and Alejandro Peralta of Caltech for NASA's Jet Propulsion Laboratory. Further information is contained in a TSP (see page 1). NPO-30576

Better Back Contacts for Solar Cells on Flexible Substrates

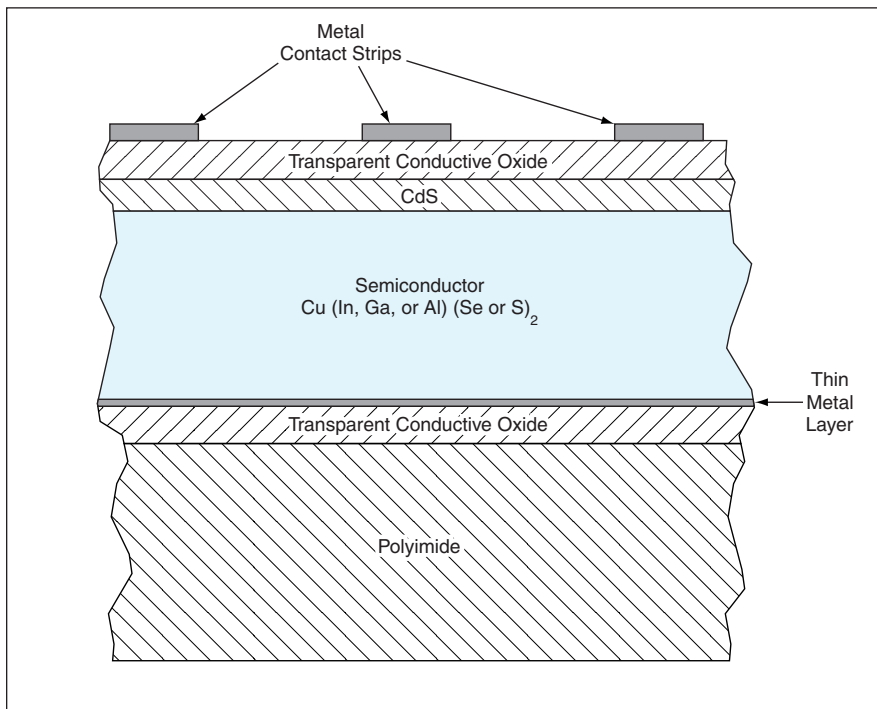
Advantages are greater efficiency and tighter adhesion.

John H. Glenn Research Center, Cleveland, Ohio

Improved low-resistance, semitransparent back contacts, and a method of fabricating them, have been developed for solar photovoltaic cells that are made

from thin films of I-III-VI₂ semiconductor materials on flexible, high-temperature-resistant polyimide substrates or superstrates. [The term "I-III-VI₂" is an abbrevi-

ated indication that the semiconductor materials are compounds of elements in periods IB, IIIA, and VIA of the periodic table in the stoichiometric ratio of 1:1:2.



The **Semitransparent Back Contact** in this device consists of the two layers between the polyimide and solar-absorber layers.

More specifically, these are compounds of general empirical formula $\text{Cu}(\text{In, Ga, or Al})(\text{Se or S})_2$.] The innovative aspect of the present development lies in the extension, to polyimide substrates or superstrates, of a similar prior development of improved low-resistance, semitransparent back contacts for I-III-VI₂ solar cells on glass substrates or superstrates. A cell incorporating this innovation can be used either as a stand-alone photovoltaic device or as part of a monolithic stack containing another photovoltaic device that utilizes light of longer wavelengths.

The figure depicts a generic device incorporating these innovations in the

substrate configuration. The semitransparent back contact that is the main focus of this article consists of two layers: The first layer deposited on the substrate is a transparent, electrically conductive oxide (for example, ZnO , InSnO_2 , or SnO_2). This layer acts mainly as a current collector. The second layer performs as contact interface layer capable of making good electrical contact with the solar-absorber material; this layer is deposited over the conductive oxide to a thickness of $<40 \text{ \AA}$.

A solar-absorber layer — a p-doped I-III-VI₂ semiconductor layer, possibly hav-

ing an n-doped surface sublayer — is grown over the thin metal layer by co-evaporation or another suitable thin-film deposition technique. Next, a layer of CdS that serves as a window and/or a heterojunction partner with the I-III-VI₂ semiconductor is deposited on the semiconductor surface by a chemical-bath or other suitable technique that does not damage the semiconductor surface. Finally, another transparent, electrically conductive oxide layer (typically of InSnO_2) that is mostly transparent to the solar spectrum is deposited over the CdS.

The semitransparency of the back contact enables the cell to function whether illuminated from the front or the back surface. Also relative to the opaque back contacts of prior such cells, the semitransparent back contact enables this cell to operate at a lower temperature, and, consequently, with greater energy-conversion efficiency. During the course of development, it was discovered that the innovative semitransparent back contact increases the adhesion between the polyimide and the solar-absorber (I-III-VI₂ semiconductor) layer — an important advantage, inasmuch as adhesion between polyimide substrates and traditional opaque molybdenum back contacts had been found to be problematic.

This work was done by Lawrence M. Woods and Rosine M. Ribelin of ITN Energy Systems, Inc., for Glenn Research Center. Further information is contained in a TSP (see page 1).

Inquiries concerning rights for the commercial use of this invention should be addressed to NASA Glenn Research Center, Commercial Technology Office, Attn: Steve Fedor, Mail Stop 4-8, 21000 Brookpark Road, Cleveland, Ohio 44135. Refer to LEW-17376.

Tunable, Highly Stable Lasers for Coherent Lidar

Designs have been refined to satisfy competing requirements for stability and tenability.

Marshall Space Flight Center, Alabama

Practical space-based coherent laser radar systems envisioned for global winds measurement must be very efficient and must contend with unique problems associated with the large platform velocities that the instruments experience in orbit. To compensate for these large platform-induced Doppler shifts in space-based applications, agile-frequency offset-locking of two single-frequency

Doppler reference lasers was thoroughly investigated. Such techniques involve actively locking a frequency-agile master oscillator (MO) source to a comparatively static local oscillator (LO) laser, and effectively producing an offset between MO (the lidar slave oscillator seed source, typically) and heterodyne signal receiver LO that lowers the bandwidth of the receiver data-collection system and permits use

of very high-quantum-efficiency, reasonably-low-bandwidth heterodyne photoreceiver detectors and circuits. Similar techniques are being applied in atmospheric CO₂ differential-absorption lidar work, where MO sources need to be actively offset-locked to CO₂ reference cells for continuous absolute-calibration purposes. Active MO/LO offset-locking is also highly applicable to lidar problems involving

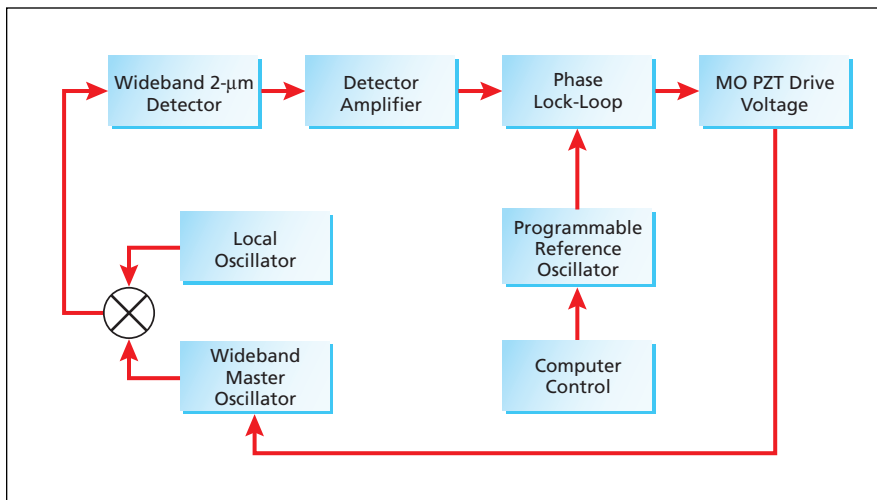


Figure 1. Tm,Ho:YLF MO/LO Offset Locking System incorporates the described improvements.

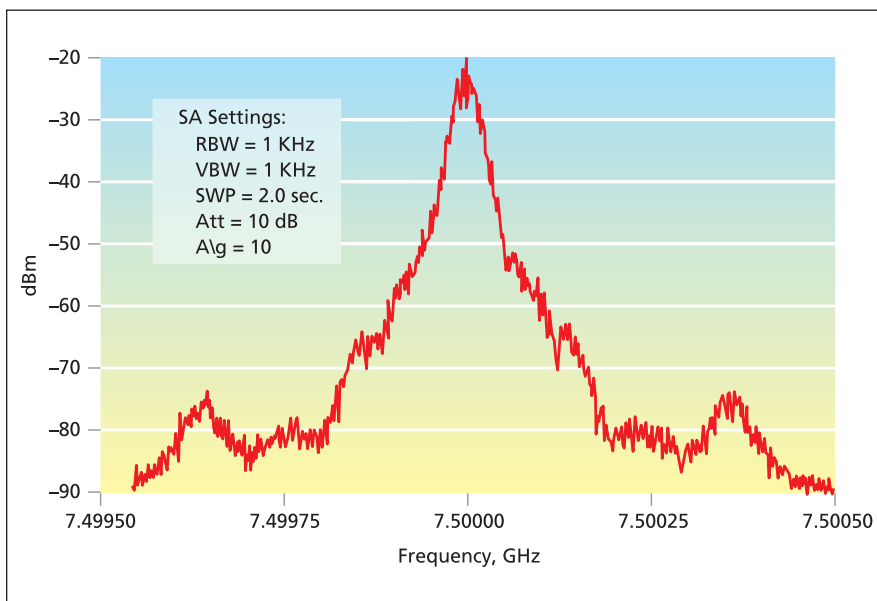


Figure 2. Heterodyne Beat Note Stability is depicted when Tm,Ho:YLF MO and LO lasers are actively offset-locked 7.5 GHz apart. Locking stability is ≈ 30 kHz over many seconds. [SA = signal analyzer; RBW = resolution bandwidth; VBW = video bandwidth; SWP = duration of frequency sweep; Att = attenuation; Alg = antenna gain.]

very high target velocities with respect to a static or moving lidar platform.

Efforts to date have focused on development of Tm,Ho:YLF lasers operating near $2.05 \mu\text{m}$, which have much poten-

tial for both efficient space-based wind lidar systems and CO_2 DIAL measurements. The locking techniques are readily applicable to any number of other wavelengths and laser formats.

Recent work on MO/LO offset locking has focused on increasing the offset locking range, improving the graded-InGaAs photoreceiver performance, and advancing the maturity of the offset locking electronics. Figure 1 provides a schematic diagram of the offset-locking system. Improvements to the design of the tunable MO laser resonator resulted in continuous, fast, SLM piezo-tuning range of 25 GHz—more than double the range of the initial prototype. Major progress was also made in the performance of very wideband, $2\text{-}\mu\text{m}$ -sensitive heterodyne photoreceivers. The fiber-coupled, hybridized-preamplifier photoreceivers developed most recently exhibited heterodyne detection bandwidth of 4 GHz to the 3 dB point, and adequate bandwidth to demonstrate robust offset-locking to 10 GHz. This advanced component is now offered as a standard product. Remarkably, these very small ($30\text{-}\mu\text{m}$ active area diameter), thin, fast PIN (positive/intrinsic/negative) devices exhibit ≈ 70 percent quantum efficiency to 4 GHz, adequate for direct use as a heterodyne receiver in many applications. With some degradation in locking robustness, MO/LO offsets of as much as 13.2 GHz were obtained. Settling times were typically 15 ms for 1 GHz steps, and locking stability was measured at 30 kHz over 20-s intervals. The system incorporated a LabVIEW-based GUI and robust auto-locking servo, greatly enhancing its usefulness in offset locking experiments and use as a wideband photoreceiver calibration instrument. Figure 2 shows a typical locking stability result.

This work was done by Sammy W. Henderson, Charley P. Hale, and David M. E'Epagnier of Coherent Technologies, Inc. for Marshall Space Flight Center. For further information, contact Kent Blanchard at ctilidar.com or (303) 379-3264. MFS-31434

Optical Profilometers Using Adaptive Signal Processing

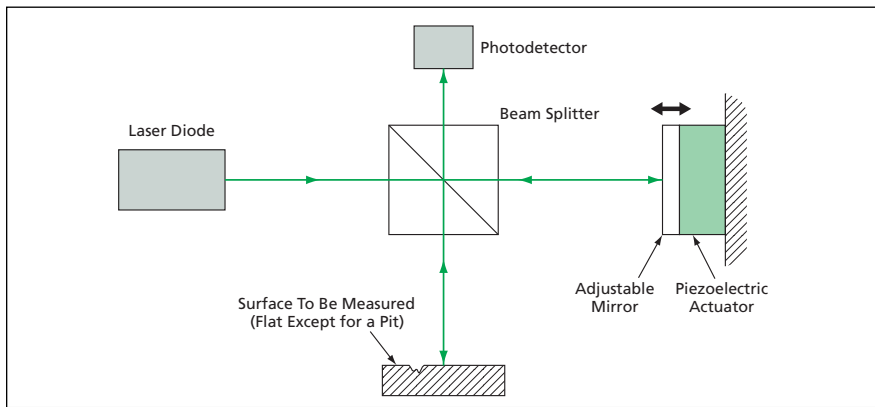
Sizes would be reduced, leading to development of hand-held profilometers.

John F. Kennedy Space Center, Florida

A method of adaptive signal processing has been proposed as the basis of a new generation of interferometric optical profilometers for measuring surfaces. Many current optical surface-measuring pro-

filometers utilize white-light-interferometry and, because of optical and mechanical components essential to their operation, are comparable in size to desktop computers. In contrast, the proposed profilome-

ters would be portable, hand-held units. Sizes could be thus reduced because the adaptive-signal-processing method would make it possible to substitute lower-power coherent light sources (e.g., laser diodes)



A Simple Michelson Interferometer could constitute the optical subsystem of a profilometer, provided that the adjustable mirror were scanned and the output of the photodetector processed as described in the text.

for white light sources and would eliminate the need for most of the optical components of current white-light profilometers. Furthermore, whereas the height scanning ranges of current surface-measuring profilometers are of the order of millimeters, the adaptive-signal-processing method would make it possible to attain scanning ranges of the order of decimeters in the proposed profilometers.

The figure depicts the optical layout of a simple Michelson interferometer configured for use as a profilometer, according to the proposal, for measuring the deviation from flatness of a nominally flat surface that contains a pit. The pit can be

characterized as comprising multiple facets at different depth, each producing a coherence function having signal intensity proportional to its size. As a result, the output of the photodetector in this interferometer would include a multitude of overlapping coherence functions that cannot be easily discriminated.

A complete overlapping-coherence-function profile of the surface area within the interrogating light beam would be collected by recording and processing the photodetector output as a function of height while scanning the adjustable mirror through the interrogation depth. The adjustable mirror could be

mounted on a piezoelectric actuator for rapid scanning in height. Optionally, a digitally controlled micromirror device could also be used to scan the light beam laterally (horizontally in the figure) across the surface. Modern digital signal-processing hardware would be used to rapidly acquire and process the photodetector output and the overlapping coherence signals contained therein according to the adaptive method described below.

In this method, a Fourier transform of a synthetic intensity-versus-depth signal generated from a mathematical model of the surface to be measured would be subtracted from the Fourier transform of the intensity-versus-depth signal obtained by the interferometer scan of the surface to be measured. The result of the subtraction would be an error signal. The coefficients of the model, representing the sizes and depths of facets in the pit, would be adjusted to minimize the error signal. To obtain the coherence function needed for the model, it would be necessary to perform a calibration measurement, prior to operation, in which a reference mirror known to be optically smooth and flat would be substituted for the surface to be measured.

This work was done by Gregory A. Hall, Robert Youngquist, and Wasfy Mikhael of Kennedy Space Center. Further information is contained in a TSP (see page 1). KSC-12647

Improved Photon-Emission-Microscope System

An advanced photon-emission microscope is combined with the latest image-processing software.

NASA's Jet Propulsion Laboratory, Pasadena, California

An improved photon-emission-microscope (PEM) instrumentation system has been developed for use in diagnosing failure conditions in semiconductor devices, including complex integrated circuits. This system is designed primarily to image areas that emit photons, at wavelengths from 400 to 1,100 nm, associated with device failures caused by leakage of electric current through SiO₂ and other dielectric materials used in multilayer semiconductor structures. In addition, the system is sensitive enough to image areas that emit photons during normal operation. This system supplants a prior PEM system based on a photon-intensified, gated, charge-coupled-device (CCD) camera.

This system includes an optical microscope fitted with a low-light-level imaging subsystem based on a state-of-the-

art high-resolution (1,024 × 1,024 pixel), cooled, back-illumination CCD camera in a light-proof enclosure. Another major subsystem is a computer running the latest in Windows-based image-processing software, which can facilitate generation of test reports and research papers by putting out image files in popular formats, including tagged image file (TIF), bit map (BMP), and Joint Photographic Experts Group (JPG) formats.

A device under test (DUT) is placed on a translation stage under the microscope. This stage enables movement of the DUT along both axes perpendicular to the optical axis, as well as along the optical axis for focusing. Any of several microscope objective lenses affording different magnifications (5×, 20×, 50×, and 100× with

extra long working distance) can be selected. The exposure time is programmable between 5 milliseconds and 2 hours. Provisions for setups of external equipment, including the power supply for the DUT and digital multimeters, can be incorporated into custom software.

In operation, the system integrates the photons emitted from the DUT, and the resulting bright spots (showing the locations of substantial emission of photons) are displayed superimposed on an image of the DUT that was acquired previously under visible light. Failure-analysis engineers can use the information in this display to locate failure sites on the DUT.

This work was done by Duc Vu of Caltech for NASA's Jet Propulsion Laboratory. Further information is contained in a TSP (see page 1). NPO-42121



Program Synthesizes UML Sequence Diagrams

A computer program called “Rational Sequence” generates Universal Modeling Language (UML) sequence diagrams of a target Java program running on a Java virtual machine (JVM). Rational Sequence thereby performs a reverse engineering function that aids in the design documentation of the target Java program. Whereas previously, the construction of sequence diagrams was a tedious manual process, Rational Sequence generates UML sequence diagrams automatically from the running Java code. Moreover, there is no need to insert instrumentation code into the target Java program. Rational Sequence employs the Java Native Interface application programming interface to create a software profiler that plugs into the JVM. Once the user starts the target Java program, Rational Sequence acts as a nonintrusive observer, generating UML diagrams representing the observed activity. Every method call, object instantiation, or thread event of the target Java program is tracked by the profiler. Once the Java program has ended, the profiler generates a UML model that contains packages, classes, and all method calls observed during the execution of the target program. The user can control the way the UML model is generated by specifying packages and/or classes to be included in the diagrams.

This program was written by Matthew R. Barry and Richard N. Osborne of United Space Alliance for Johnson Space Center. For further information, contact the Johnson Technology Transfer Office at (281) 483-3809. MSC-23656

Aspect-Oriented Subprogram Synthesizes UML Sequence Diagrams

The Rational Sequence computer program described in the immediately preceding article includes a subprogram that utilizes the capability for aspect-oriented programming when that capability is present. This subprogram is denoted the Rational Sequence (As-

pectJ) component because it uses AspectJ, which is an extension of the Java programming language that introduces aspect-oriented programming techniques into the language. The Rational Sequence (AspectJ) component is compiled with a target Java application program on an AspectJ compiler. The user then starts the Java application program. Thereafter, the Rational Sequence (AspectJ) component publishes every visible method call to a Universal Modeling Language (UML) sequence diagram. When the Java application program ends, a sequencer proceeds to generate a UML model that contains packages, classes, and all method calls that occurred during the execution of the program. The user can control the way the UML model is generated by specifying, via the aspect source code, packages and/or classes to be included in the diagrams. Like the rest of Rational Sequence, the AspectJ component complies with the UML specification.

This program was written by Matthew R. Barry and Richard N. Osborne of United Space Alliance for Johnson Space Center. For further information, contact the Johnson Technology Transfer Office at (281) 483-3809. MSC-23655

Updated Computational Model of Cosmic Rays Near Earth

An updated computational model of the galactic-cosmic-ray (GCR) environment in the vicinity of the Earth, Earth’s Moon, and Mars has been developed, and updated software has been developed to implement the updated model. The GCR model and software in their original forms, developed during the early 1990s, were based on balloon and satellite data from 1954 to 1992. This model accounts for solar modulation of the cosmic-ray contribution for each element from hydrogen through iron by computationally propagating the local interplanetary spectrum of each element through the heliosphere. The propagation is effected by solving the Fokker-Planck diffusion, convection, energy-loss boundary-value problem.

Since August 1997, the Advanced Composition Explorer NASA satellite has provided new data on GCR energy spectra. These new data were used to update the original model and greatly improve the accuracy of prediction of interplanetary GCR. The updated software was also simplified significantly, relative to the original software. The updated model and software are expected to provide highly accurate GCR-environment data for use by interplanetary-mission planners in planning for protecting astronauts against radiation and ensuring radiation hardness of electronic equipment.

This program was written by Patrick M. O’Neill of Johnson Space Center. For further information, contact the Johnson Technology Transfer Office at (281) 483-3809. MSC-23891

Software for Alignment of Segments of a Telescope Mirror

The Segment Alignment Maintenance System (SAMS) software is designed to maintain the overall focus and figure of the large segmented primary mirror of the Hobby-Eberly Telescope. This software reads measurements made by sensors attached to the segments of the primary mirror and from these measurements computes optimal control values to send to actuators that move the mirror segments. The software also acts as a logger for the collected data, a server from which the hardware of the control computer can acquire control information and other computers can collect data, and a monitoring and diagnostic system. The software provides a graphical user interface through which human operators can exert control. The software supports four modes of operation:

- *Operate* — The server acquires the sensory data and processes them into commands for the actuators.
- *Calibrate* — Calibration tests are performed on the edge sensors and the relationships between actuator commands and sensor responses are quantified.
- *Standby* — The server is initialized in standby mode, from which it can

make the transition to any of the other three modes.

- *Diagnostic* — This mode provides access to all sensory data in real time and is intended for use in diagnosis of sensor anomalies.

This program was written by Drew P. Hall, Richard T. Howard, William C. Ly, John M. Rakoczy, and John M. Weir of Marshall Space Flight Center. For further information, contact Jim Dowdy, Commercialization Project Lead, at Jim.Dowdy@nasa.gov. MFS-31835-1

Simulation of Dropping of Cargo With Parachutes

Decelerator System Simulation (DSS) is a computer program for predicting and analyzing the dynamics of a load of cargo dropped with parachutes from an aircraft. A DSS simulation runs from the first motion in the aircraft until the payload reaches the ground. Intended for use in support of airdrop tests for the X-38 program, DSS was developed by modifying and augmenting an older program, denoted UD233A, used for simulating the dynamics of a space-shuttle solid rocket booster falling with a parachute. The main effort in converting UD233A into DSS involved development of computational models for simulating the inflation of one or more parachute(s), the dynamics of the payload and the slings connecting the parachute(s) with the payload, and the extraction of the payload and parachutes from the aircraft.

This program was written by Peter Cuthbert of Johnson Space Center. For further

information, contact the Johnson Technology Transfer Office at (281) 483-3809. MSC-2363

DAVE-ML Utility Programs

DAVEtools is a set of Java archives (*.jar files) that embodies tools for manipulating flight-dynamics models that have been encoded in dynamic aerospace vehicle exchange markup language (DAVE-ML). [DAVE-ML is an application program, written in Extensible Markup Language (XML), for encoding complete computational models of the dynamics of aircraft and spacecraft. The goal in the continuing development of DAVE-ML is to expedite the exchange and validation of dynamical models, via the Internet, in a manner that is consistent and is independent of computational-simulation facilities, computing languages, and simulation software.] At present, *DAVEtools* includes two tools:

- *dave* (a basic DAVE-ML parser), which generates a Java-based version of a model encoded in DAVE-ML and
- *dave2sl*, which builds on *dave* to create Simulink® representations of models encoded in DAVE-ML.

The manipulations that can be performed at the present early stage of development are rather limited. More importantly, *DAVEtools* serves as an example of how to write an import software tool for a DAVE-ML file.

This program was written by Bruce Jackson of Langley Research Center. For further information, access <http://daveml.nasa.gov>. LAR-16879-1

Robust Control for the Mercury Laser Altimeter

Mercury Laser Altimeter Science Algorithms is a software system for controlling the laser altimeter aboard the Messenger spacecraft, which is to enter into orbit about Mercury in 2011. The software will control the altimeter by dynamically modifying hardware inputs for gain, threshold, channel-disable flags, range-window start location, and range-window width, by using ranging information provided by the spacecraft and noise counts from instrument hardware. In addition, because of severe bandwidth restrictions, the software also selects returns for downlink. To reduce mission risk, the software incorporates three different modes of operation. The three modes are denoted as fixed, range-driven, and closed-loop (or adaptive). The fixed mode provides fixed hardware inputs for all but the threshold. The range-driven mode receives and utilizes ranging information from the spacecraft regarding its slant range to the planet or asteroid. The adaptive mode is capable of improving upon the ranging information provided by the spacecraft by use of a closed-loop range-estimation algorithm. The software is sufficiently robust that it could be used on other missions, and in fact, this has already been proposed.

This program was written by Jacob S. Rosenberg of Goddard Space Flight Center. Further information is contained in a TSP (see page 1). GSC-14876-1



Thermally Stable Piezoelectric and Pyroelectric Polymers

Neither mechanical nor solvent treatment is necessary for orientation of polymer molecules.

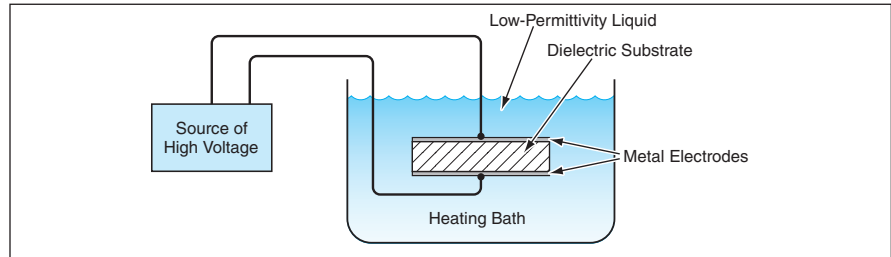
Langley Research Center, Hampton, Virginia

A class of thermally stable piezoelectric and pyroelectric polymers, and an improved method of making them, have been invented. These polymers can be used as substrates for a wide variety of electromechanical transducers, sensors, and actuators.

In order to enable a material to produce an electrostatic potential in response to mechanical excitation (piezoelectricity) or in response to thermal excitation (pyroelectricity), the material must be electrically polarized; that is, its molecules must be at least partially aligned in a preferred electric-dipole orientation. The preferred orientation or polarization occurs naturally in quartz and some crystalline materials, and can be induced in some ceramics and polymers by application of strong electric or mechanical fields.

Prior to this invention, poly(vinylidene fluoride) [PVF₂] was the only commercially available piezoelectric polymer. In order to be able to exploit the piezoelectricity of PVF₂, it was necessary to orient its molecules by mechanical drawing of sheets or by dissolving the PVF₂ in a solvent and then subjecting it to an electric field while causing the solvent to evaporate. In contrast, the polymers of the present invention are rendered piezoelectric and/or pyroelectric by means of an orientation process that does not involve either a solvent or a mechanical treatment.

The polymers suitable for this invention include polyarylates, polyquinoxalines, polyphenylene ethers, polycarbonates, polyphenylene sulfides, polysulfones, polyaryletherketones, polyimides, polyarylene ethers, polybenzimidazoles,



A Polymer Substrate Is Heated to its softening temperature in a low-permittivity dielectric liquid while a high voltage is applied to metal electrodes on opposite faces to induce electric polarization. When the electrode/substrate/electrode sandwich is cooled, the polarization remains frozen into the substrate.

polyazomethines and possibly other thermally stable polymers. These polymers have softening temperatures greater than about 100 °C, and, once polarized, they retain their polarizations (and, hence, their piezoelectric and pyroelectric properties) at temperatures up to their softening temperatures.

A polymeric substrate to be rendered piezoelectric and/or pyroelectric according to the invention is prepared by depositing metal electrodes on opposite faces. The electrode metal can be gold, silver, or any other suitable low-electrical-resistivity metal that is not readily oxidized at the temperature to be used in the treatment described next. The metal electrodes are connected to a source of high voltage, and the electrode/substrate/electrode sandwich is immersed in a heating bath containing silicone oil or other suitable low-permittivity dielectric liquid (see figure). In the bath, the electrode/substrate/electrode sandwich is heated to the softening temperature of the polymer to increase the mobility of the polymer molecules. A voltage is

applied to the electrodes to generate an electric field (typically between 50 and 200 MV/m) large enough to orient the polymer molecules but not so large as to cause dielectric breakdown of the polymer substrate. The voltage can be low-frequency AC or DC. The voltage is maintained for an interval of time sufficient to obtain the desired degree of polarization. The electrode/substrate/electrode sandwich is then cooled while maintaining the voltage. Once the temperature is well below the softening temperature, the voltage is turned off, and the induced orientation remains frozen into the polymer.

This work was done by Joycelyn O. Simpson and Terry L. St. Clair of Langley Research Center. Further information is contained in a TSP (see page 1).

This invention has been patented by NASA (U.S. Patent Nos. 5,891,581, 5,909,905, and 6,379,809). Inquiries concerning nonexclusive or exclusive license for its commercial development should be addressed to the Patent Counsel, Langley Research Center, at (757) 864-3521. Refer to LAR-15279.

Combustion Synthesis of Ca₃(PO₄)₂ Net-Shape Surgical Implants

More-biocompatible materials are produced in fewer processing steps.

John H. Glenn Research Center, Cleveland, Ohio

Self-propagating high-temperature combustion synthesis (SHS) is the basis of a method of making components of porous tricalcium phosphate [Ca₃(PO₄)₂] and related compounds in net sizes and

shapes for use as surgical implants that are compatible with bone. Ca₃(PO₄)₂-based materials are among those preferred for use in orthopedic, restorative, and reconstructive surgery. As explained

below, the SHS method offers advantages over prior methods of manufacturing Ca₃(PO₄)₂-based surgical implants.

Ca₃(PO₄)₂ occurs in at least two crystalline forms: a monoclinic form de-

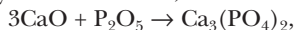
noted the α phase and an orthorhombic form denoted the β phase. The β phase is the preferred form for bone replacement because it can be resorbed by the body, facilitating bone remodeling. At an appropriate porosity, β $\text{Ca}_3(\text{PO}_4)_2$ resembles natural bone and serves as a scaffold into which osteogenic cells can migrate. Thus, bone becomes directly attached to and grows into a β $\text{Ca}_3(\text{PO}_4)_2$ implant. The body generally resorbs β $\text{Ca}_3(\text{PO}_4)_2$ within about two years, replacing it with natural bone.

Prior methods of making surgical implants of $\text{Ca}_3(\text{PO}_4)_2$ and related materials have not yet been perfected. The prior methods involve, variously, synthesis of $\text{Ca}_3(\text{PO}_4)_2$ -containing bioceramics from aqueous solutions, sintering, sol-gel processing, and/or casting of polymeric foams mixed with slurries of $\text{Ca}_3(\text{PO}_4)_2$ -containing bioceramic particles. All of these prior methods are energy- and labor-intensive, and each requires several time-consuming steps. Of particular interest is the sintering method, which includes molding by compacting a powder into a die having the size and shape of the desired part, then heating to temperature just high enough that the powder particles undergo solid-state bonding to each other but do not melt. The great disadvantage of this method is that at the high sintering temperature, β $\text{Ca}_3(\text{PO}_4)_2$ becomes converted to α $\text{Ca}_3(\text{PO}_4)_2$, which is not preferable as a bone replacement material.

Relative to any of the prior methods, the present SHS-based method requires

fewer steps, takes less time, enables better tailoring of porosity, and yields a greater ratio between the desired β phase and the undesired α phase. Processing according to this method begins with preparation of a mixture of CaO and P_2O_5 powders and possibly other ingredients described below. Processing must be done in a protective dry, nonreactive atmosphere (e.g., argon) because P_2O_5 is hygroscopic and strongly reactive. The mixture is compacted into a combustible or noncombustible die having the size and shape of the desired part. If the die is noncombustible, the preform of compacted powder is then removed from the die carefully so as not to deform or break it.

Next, the compacted powder preform is heated to initiate the main combustion synthesis reaction,



which is accompanied by some other reactions that yield a variety of calcium-, oxygen-, and phosphorus-containing byproducts. The main combustion synthesis reaction is exothermic and self-sustaining: once it has been initiated, a wavefront comprising a reaction zone moves through the mixture. In the reaction zone and its vicinity, the reactant having the lowest melting temperature momentarily spreads by means of capillary action, leading to a large dispersion of the reaction products.

In general, $\text{Ca}_3(\text{PO}_4)_2$ is formed if the mixture contains between about 60 and 90 mole percent of CaO and between about 10 and 40 mole percent of P_2O_5 .

The proportions of these ingredients can be adjusted to tailor the proportions of the α and β phases of $\text{Ca}_3(\text{PO}_4)_2$ in the combustion-synthesis product. Optionally, the reaction mixture can include one or more dopants and/or a gasifying agent. Also optionally, the combustion-synthesis product can be subjected to a further process of controlled heating and cooling to increase the ratio between the β and α phases of $\text{Ca}_3(\text{PO}_4)_2$.

Process parameters can also be varied to tailor the degree of porosity, the proportion of interconnected pores, and the shapes of the pores in the finished product, and to impart functionally graded porosity as might be required for a particular application. Examples of such parameters include, but are not limited to, the pressure used to compact the reactant mixture, the amount of the gasifying agent, the proportions of CaO and P_2O_5 in the reactant mixture, the sizes of the reactant powder particles, and the pressure of the atmosphere in which the reaction takes place.

This work was done by Reed A. Ayers, Martin Castillo, Guglielmo Gottoli, John J. Moore, and Steven J. Simske of the Colorado School of Mines for Glenn Research Center. Further information is contained in a TSP (see page 1).

Inquiries concerning rights for the commercial use of this invention should be addressed to NASA Glenn Research Center, Innovative Partnerships Office, Attn: Steve Fedor, Mail Stop 4-8, 21000 Brookpark Road, Cleveland, Ohio 44135. Refer to LEW-17951-1.



Stochastic Representation of Chaos Using Terminal Attractors

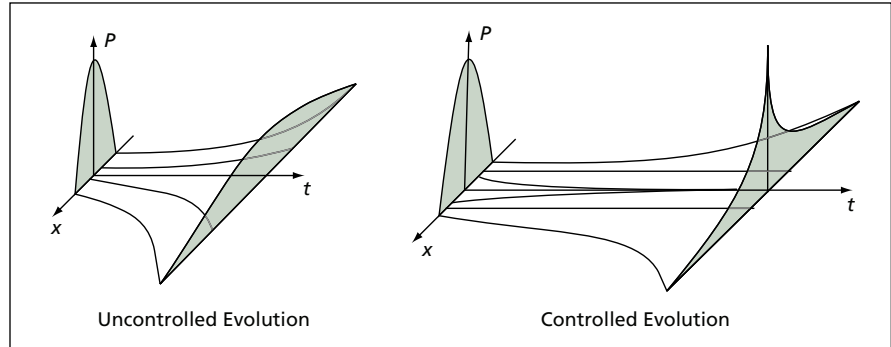
Fictitious control forces stabilize what would otherwise be unstable computed trajectories.

NASA's Jet Propulsion Laboratory, Pasadena, California

A nonlinear version of the Liouville equation based on terminal attractors is part of a mathematical formalism for describing postinstability motions of dynamical systems characterized by exponential divergences of trajectories leading to chaos (including turbulence as a form of chaos). The formalism can be applied to both conservative systems (e.g., multibody systems in celestial mechanics) and dissipative systems (e.g., viscous fluids).

This formalism at an earlier stage of development was reported in "Extension of Liouville Formalism to Postinstability Dynamics" (NPO-30393), NASA Tech Briefs, Vol. 27, No. 9 (September 2003), page 56. To recapitulate: The problem is to predict the postinstability motions of a dynamic system governed by a system of nonlinear equations and subject to initial conditions. The formalism of nonlinear dynamics does not afford means to discriminate between stable and unstable motions: an additional stability analysis is necessary for such discrimination. However, an additional stability analysis does not suggest any modifications of a mathematical model that would enable the model to describe postinstability motions efficiently. The most important type of instability that necessitates a postinstability description is associated with positive Lyapunov exponents. Such an instability leads to exponential growth of small errors in initial conditions or, equivalently, exponential divergence of neighboring trajectories.

The development of the present formalism was undertaken in an effort to remove positive Lyapunov exponents. The means chosen to accomplish this is coupling of the governing dynamical equations with the corresponding Liouville equation that describes the evolution of the flow of error probability. The underlying idea is to suppress the divergences of different trajectories that correspond to different initial conditions, without affecting a target trajectory, which is one that starts with prescribed initial conditions.



The Probability Distribution of Error about a target trajectory becomes flattened in uncontrolled evolution as close neighboring trajectories diverge. However, when evolution is controlled by fictitious stabilizing forces that create a terminal attractor in probability space, the distribution of error becomes more sharply peaked about the target trajectory.

This formalism applies to a system of n first-order ordinary differential equations in n unknown dynamical (state) variables:

$$\dot{x}_i = f_i[\mathbf{x}(t), t],$$

where i is an integer between 1 and n , x_i is one of the unknown dynamical variables, the overdot signifies differentiation with respect to time, \mathbf{x} is the vector of all the dynamical variables (x_1, x_2, \dots, x_n) , and t is time. The prescribed initial conditions are given by

$$x_i = x_i^0,$$

The corresponding Liouville equation for the evolution of the probability distribution, $P(x_1, x_2, \dots, x_n, t)$, of errors in the initial conditions is

$$\frac{\partial P}{\partial t} + \nabla \cdot (P\mathbf{f}) = 0$$

where \mathbf{f} is the vector of all the forcing functions (f_1, f_2, \dots, f_n) . It is assumed that this probability distribution peaks at zero error (representing the prescribed initial conditions).

Fictitious control (stabilizing) forces $[\mathbf{F} = (F_1, F_2, \dots, F_n)]$ are added to the system of differential equations. The form of these forces differs from that of the fictitious stabilizing force described in the cited previous article: Whereas previously, the fictitious stabilizing force was proportional to the gradient of the probability density in the space of the dynamical variables,

the present fictitious control forces are functions of the differences between expected and actual values of the dynamical variables x_i :

$$F_i \equiv \gamma_i \left(\langle x_i \rangle - x_i \right)^{\frac{1}{3}}$$

where γ_i is a positive constant and $\langle x_i \rangle$ is the expected value of x_i , as given by

$$\langle x_i \rangle = \int_{-\infty}^{\infty} X_i P dX_1 \dots dX_n$$

The control forces have two important properties:

- Because they vanish as $\mathbf{x} \rightarrow \langle \mathbf{x} \rangle$, they do not affect the target trajectory; and
- Because the magnitudes of their derivatives approach ∞ as $\mathbf{x} \rightarrow \langle \mathbf{x} \rangle$, they make the target trajectory infinitely stable. In other words, the target trajectory becomes a terminal attractor.

The resulting modified system of dynamical equations is

$$\dot{x}_i = f_i + \gamma_i \left(\langle x_i \rangle - x_i \right)^{\frac{1}{3}}$$

The corresponding modified Liouville equation is

$$\frac{\partial P}{\partial t} = - \sum_{i=1}^n \frac{\partial}{\partial x_i} \left\{ P \left[f_i + \gamma_i \left(\langle x_i \rangle - x_i \right)^{\frac{1}{3}} \right] \right\},$$

wherein the terminal attractors act as nonlinear sinks of probability.

At the limit as $x_i \rightarrow \langle x_i \rangle$, one can neglect the real force f_i as being much smaller than the control force F_i , making it possible to decompose the Liouville equation

into n independent equations and to express P as a product of n probabilities P_i :

$$\frac{\partial P_i'}{\partial t} = -\gamma_i \frac{\partial P_i'}{\partial x_i} \left((x_i) - x_i \right)^{\frac{1}{3}} \text{ and}$$

$$P(x_1, x_2, \dots, x_n) = \prod_{i=1}^n P_i'(x_i)$$

By use of these equations, it can be shown that the control forces create a powerful terminal attractor in probabilistic space that corresponds to occur-

rence of the target trajectory with probability one (see figure). In configuration space (space in the sense in which "space" is understood in casual conversation), the effect of the control forces is to suppress exponential divergence of close neighboring trajectories without affecting the target trajectory. As a result, the post-instability motion is represented by a set of functions that describe the evolution of such statistical invariants such as expectations, vari-

ances, and higher moments of the statistics of the state variables x_i as functions of time.

This work was done by Michail Zak of Caltech for NASA's Jet Propulsion Laboratory. Further information is contained in a TSP (see page 1).

The software used in this innovation is available for commercial licensing. Please contact Karina Edmonds of the California Institute of Technology at (818) 393-2827. Refer to NPO-41519.

Two High-Temperature Foil Journal Bearings

These are prototypes of foil bearings for aircraft gas turbine engines.

John H. Glenn Research Center, Cleveland, Ohio

An enlarged, high-temperature-compliant foil bearing has been built and tested to demonstrate the feasibility of such bearings for use in aircraft gas turbine engines. At 150 mm in diameter, this is the largest foil bearing known to date. This bearing is a scaled-up version of a patented 100-mm-diameter foil bearing, augmented by coating the foil with a proprietary high-temperature material. In a companion development, a foil bearing as described above has been combined with a 150-mm-diameter active magnetic bearing to make a hybrid foil magnetic bearing.

Foil bearings are attractive for use in some machines in which (1) speeds of rotation, temperatures, or both exceed maximum allowable values for rolling-element bearings; (2) conventional lubricants decompose at high operating temperatures; and/or (3) it is necessary or desirable not to rely on conventional lubrication systems. In a foil bearing, the lubricant is the working fluid (e.g., air or a mixture of combustion gases) in the space between the journal and the shaft in the machine in which the bearing is installed. At no or low speed, the shaft is supported at by a spring-loaded foil journal lining. Once the shaft is rotating rapidly enough, the hydrodynamic and viscous forces exerted by the flow of working fluid between the foil and the shaft force the foil away from the shaft, so that the shaft becomes supported by a film of the working fluid.

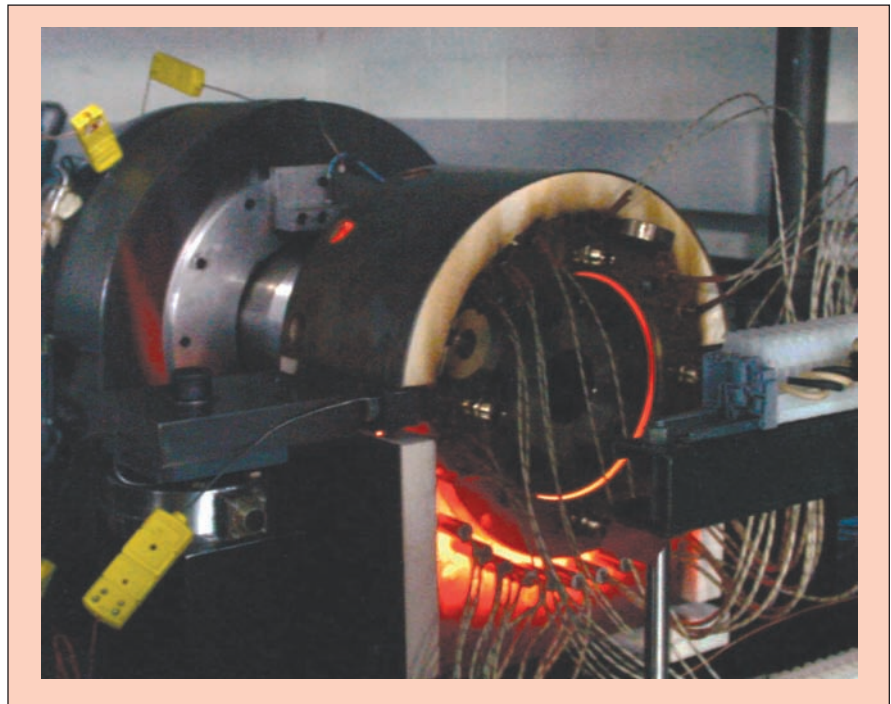
The present enlarged, high-temperature foil bearing has been tested at speeds up to 27,000 rpm (at 150 mm diameter, corresponding to a surface speed of 212 m/s) and at temperatures

in excess of 1,200 °F (>649 °C). These speed and temperature limits exceed those of rolling-element bearings by several fold.

The hybrid foil magnetic bearing was conceived to take advantage of the strengths of the foil and the active magnetic bearing while utilizing each bearing to compensate for the weakness of the other, for the overall purpose of obtaining high load capacity at all speeds and temperatures (see figure). The active magnetic bearing exhibits excellent performance at low speed, where the surface coating on the foil bearing has limited load capacity. The foil bearing

exhibits excellent performance at high speed, where the active magnetic bearing can fail in response to shocks and other transient disturbances.

Unlike a conventional active magnetic bearing, the hybrid foil magnetic bearing can operate without need for a separate protective auxiliary/backup bearing. In case of failure of the active magnetic bearing in the hybrid foil magnetic bearing, the foil bearing plays the role of the backup bearing, so that a rotor can continue to run on the foil bearing alone and then come down to a safe stop. The hybrid foil magnetic bearing exhibits both the high load ca-



The Hybrid Foil Magnetic Bearing was photographed in operation at a speed of 15,000 rpm at a temperature of 1,200 °F (>649 °C)

capacity of the foil bearing and the high static stiffness and control versatility of the active magnetic bearing. Hence, the hybrid foil magnetic bearing system implements a significant advance in range of operation and reliability.

This work was done by Hooshang Heshmat of Mohawk Innovative Technology, Inc. for Glenn Research Center. Further information is contained in a TSP (see page 1).

Inquiries concerning rights for the commercial use of this invention should be addressed

to NASA Glenn Research Center, Innovative Partnerships Office, Attn: Steve Fedor, Mail Stop 4-8, 21000 Brookpark Road, Cleveland, Ohio 44135. Refer to LEW-17643-1.

Using Plates To Represent Fillets in Finite-Element Modeling

Structural deflections are approximated by use of simplified computational submodels of fillets.

Marshall Space Flight Center, Alabama

A method that involves the use of fictitious plate elements denoted bridge plates has been developed for representing the stiffnesses of fillets in finite-element calculations of deflections, stresses, and strains in structures. In the absence of this method, it would be necessary to either neglect the effects of fillets to minimize the computational burden or else incur a large computational burden by using complex computational models to represent the fillets accurately. In effect, the bridge plates of the present method are reduced-order models of fillets that do not yield accurate stresses within fillets but do make it possible to accurately calculate the dynamic characteristics of the structure and to approximate the effects of fillets on stresses and strains elsewhere in a structure that contains the fillets. Such approximations are accurate enough for final modal analysis and preliminary stress analyses.

In a finite-element model according to this method, the model of a fillet includes bridge plates that connect the tangent lines of the fillets. For a given fillet, the bridge plates are characterized by a thickness (t_b) and a pseudo Young's modulus (E_b) to represent the mass and stiffness of the fillet as accurately as possible. It is necessary to calculate t_b and E_b in advance, by means of the procedure described in the next paragraph.

One generates two simultaneous nonlinear wide-beam-deflection equations for the rotation at the tangent lines: an equation applicable to the bridge-plate representation and an equation derived from an analytic representation of the fillet. These equations are formulated in terms of the independent variables r/t and t_{wall}/t , where r is the fillet radius, t_{wall} is the thickness of the non-filletted section of a wall adjacent to the filleted section,

and t is a thickness variable, the value of which one seeks. The equations are solved numerically to obtain t_b and E_b . In addition, surface fits of the solutions are obtained for use as the equivalent of closed-form equations for t_b and E_b .

The method has been verified in calculations pertaining to a representative filleted structure. The bridge-plate model yielded a level of accuracy for the calculation of natural frequencies and mode shapes better than or equal to that obtained by use of a high-fidelity solid model of the fillet, even though the bridge-plate model contained 90 percent fewer degrees of freedom.

This work was done by Andrew Brown of Marshall Space Flight Center. For further information, access the Technical Support Package (TSP) free on-line at www.techbriefs.com/tsp under the Mechanics category. MFS-31992



Repairing Chipped Silicide Coatings on Refractory Metal Substrates

Two methods have been demonstrated to be feasible.

John F. Kennedy Space Center, Florida

The space shuttle orbiter's reaction control system (RCS) is a series of small thrusters that use hypergolic fuels to orient the orbiter in space. The RCS thrusters are constructed from a special niobium-based alloy — the C-103. This alloy retains excellent mechanical properties from cryogenic temperature all the way up to 2,500 °F (1,370 °C). Despite its excellent, high-temperature properties, C-103 is susceptible to rapid oxidation at elevated temperatures. Were the naked C-103 alloy exposed to the operational thruster environment, it would rapidly oxidize, at least losing all of its structural integrity, or, at worst, rapidly “burning.” Either failure would be catastrophic. To prevent this rapid oxidation during thruster firing, the RCS thrusters are coated with a silicide-based protective coating — the R512a. Over time, this protective coating becomes weathered and begins to develop chips. Launch Commit Criteria limit the diameter and depth of an acceptable pit; otherwise, the thruster must be removed from the orbiter — a very costly, time-consuming procedure. The authors have developed two methods to repair damaged R512a coatings on C-103.

For the first repair technique, metal foundries, semiconductor manufacturers, and many other industries have developed and routinely use coatings that can easily be painted on metal to protect it from corrosion, including oxidation, to temperatures in excess of 2,500 °F (1,370 °C). These coatings are typically a well-chosen oxide in a special organic binder that adheres to metallic surfaces. The organic binder is se-

lected, so that upon exposure to elevated temperature, the ceramic is held in proximity to the substrate and forms somewhat of a chemical bond to the surface. If the binder is freed from the surface, the ceramic deposit remains and maintains an effective oxygen barrier. Commercially available, off-the-shelf ceramic paints may be used to repair chipped R512a and protect the underlying C-103 from subsequent oxidation. The authors have identified several candidates that aid in the protection of C-103. This first repair technique is considered somewhat temporary. The ideal use for the ceramic paints would be to repair an RCS nozzle when a chip is discovered, say, at the launch pad. It would serve as a protective coating for at least one mission, prevent the rollback of the shuttle, and postpone the replacement of the nozzle until a more opportune time in the ground-processing flow.

The second repair technique is based on using the native coating material of the RCS nozzles. In this case, the chipped area is ground out and a “green” R512a coating is applied to the repair area. After the green coating has dried, it must be heated at extreme elevated temperatures while in vacuum or inert atmosphere to initiate the solid-state reaction between the R512a and the C-103. In the early 80's, a repair process was developed using a variant of the native coating and a focused quartz lamp to heat the local area. Due to the bulky size of the lamp and focusing assembly, only the areas along the outer periphery of the nozzles could be repaired. The authors have devel-

oped a technique using a fiber-coupled, high-powered laser as heat source to successfully fuse the green R512a to C-103. The resulting repaired areas on test coupons are chemically and structurally equivalent to the native coated areas. Since the fiber-coupled laser assembly is quite small and easy to handle, all areas of the nozzle are accessible for repair, including the throat area. Since this repair technique results in a protective barrier that is equivalent to the original coating, it is considered to be a permanent repair. Thermal modeling and calculations have shown that during the fusing process, all other areas of the nozzle remain within specifications, so that the processes are viable *in situ* on actual thrusters, although not while they are installed on the orbiter.

The two techniques are complementary in the sense that the ceramic paints are easily applied and do not require excessive temperatures. While not as desirable as the permanent repair, they could be applied for moderate protection until the permanent laser-repair technique is available to the repair area. Both repair techniques were originally intended for RCS nozzles, but the process could easily be applied to other geometries of R512a/C-103. Additionally, the two repair techniques may be adapted to other high-temperature coating/substrate systems.

This work was done by Robert Youngquist of Kennedy Space Center and Christopher D. Immer and Francisco Lorenzo-Luaces of ASRC Aerospace. Further information is contained in a TSP (see page 1). KSC-12690/29

Simplified Fabrication of Helical Copper Antennas

From concept to working prototype takes just a few hours.

Lyndon B. Johnson Space Center, Houston, Texas

A simplified technique has been devised for fabricating helical antennas for use in experiments on radio-frequency generation and acceleration of plasmas.

These antennas are typically made of copper (for electrical conductivity) and must have a specific helical shape and precise diameter.

Such an antenna could be made by bending a single long piece of copper tubing or bending smaller pieces of copper tubing, then welding the pieces to-

gether. It could also be made by machining from a single large piece of copper. It is extremely difficult to bend copper tubing into a helix with a precise pitch and diameter. It is also difficult to create the helical shape from multiple pieces of tubing; moreover, welding separate pieces distorts the shape. Machining a hollow cylindrical helix from a block or cylinder of copper entails the use of a complex, expensive, three-dimensional-milling machine in a process that entails long setup and machining times.

In the present simplified technique, one begins by creating a two-dimensional paper template of a desired helical antenna shape. The template is pasted on the outer surface of a copper pipe that has the desired inner and outer diam-

eters. Holes are drilled at the locations where corners are required to exist in the final helical antenna. Manually, using a hacksaw, diagonal cuts are made in the outer cylindrical surface of the pipe, following the lines on the template. Usually, after hacksawing, only a little filing is needed to smooth the edges of the resulting antenna. If the antenna must be water-cooled, then copper tubing can be brazed onto the outer surface of the antenna. This tubing is not required to follow the precisely defined shape of the antenna.

This fabrication technique would not be suitable for mass production, but it is ideal for a laboratory environment. The advantages of the this technique are the following:

- Precise antennas can be made from inexpensive, stock-size copper pipes.
- No welding of separate pieces is needed, and so there is no welding-induced distortion of antenna shapes.
- Prototype antennas can be fabricated fairly rapidly, without the need for complex three-dimensional-milling machines or computer-aided drafting tools.
- Notwithstanding the reliance on handwork, the total fabrication time (as little as a few hours) is competitive with, and probably less than, that of any automated process that could be used for this purpose.

This work was done by Andrew Petro of Johnson Space Center. Further information is contained in a TSP (see page 1).

MSC-24076



Graded-Index “Whispering-Gallery” Optical Microresonators

Improvements would include equidistant resonances and reduced evanescent field.

NASA's Jet Propulsion Laboratory, Pasadena, California

Graded-index-of-refraction dielectric optical microresonators have been proposed as a superior alternative to prior dielectric optical microresonators, which include microspheres (described in several prior *NASA Tech Briefs* articles) and microtori wherein electromagnetic waves propagate along circumferential paths in “whispering-gallery” modes. The design and method of fabrication of the proposed microresonators would afford improved performance by exploiting a combination of the propagation characteristics of the whispering-gallery modes and the effect of a graded index of refraction on the modes.

The prior microresonators have been shown to be capable of functioning as compact, high-performance optical filters characterized by rarefied spectra of narrow resonance lines. For many applications, the frequency intervals between resonances are required to be equal. Unfortunately, the techniques used to fabricate the prior microresonators cannot be used to obtain equidistant resonances. The variation of frequency spacing of resonances is a consequence of the frequency dependence of the radial distribution of the whispering-gallery resonant modes: In a given microresonator that does not have a graded index of refraction, higher-frequency modes propagate on paths slightly closer to the surface, relative to lower-frequency modes. In other words, the higher-frequency modes propagate circumferentially at slightly larger radii and, consequently, slightly longer

optical path lengths. The variation of optical path lengths results in nonuniform spacing of resonance frequencies.

Optical path length is a function of both distance (in the common geometrical sense) and the index of refraction. A microresonator according to the proposal would be fabricated from a graded-index-of-refraction cylinder. The parameters of the fabrication process would be chosen such that the index of refraction of the cylinder would decrease with radius by an amount calculated on the basis of the propagation characteristics of the desired resonances. Although higher-frequency modes would still travel geometrically longer distances, the indices of refraction at the larger radii would be lower (the waves would travel faster). With proper choice of the rate of decrease of the index of refraction with radius, the circumferential paths at all radii would have identical optical path lengths and consequently, to first order, the resonances would be equidistant in frequency.

Additional potential advantages of the proposal include the following:

- Fabrication should be straightforward: Graded-index-of-refraction optical components are widely available in the form of lenses and optical fibers. Such components can be formed into microresonators by use of standard mechanical and flame-polishing techniques.
- The proposed grading of indices of refraction would push the whispering-

gallery modes slightly deeper into the resonator material, so that the evanescent fields would be smaller. As a result, losses attributable to imperfections of surfaces would be less than in the prior microresonators.

- The designs of the prior microresonators exploit evanescent-field coupling via airgaps. Vibrations give rise to small changes in the airgaps, thereby causing fluctuations in coupling strength. In the proposed microresonators, the greater depth of propagation of the resonant modes would make it possible to use zero-gap coupling, so that vibration would no longer cause fluctuations in the strengths of coupled optical signals.

This work was done by Anatoliy Savchenkov, Lute Maleki, Vladimir Ilchenko, and Andrey Matsko of Caltech for NASA's Jet Propulsion Laboratory. Further information is contained in a TSP (see page 1).

In accordance with Public Law 96-517, the contractor has elected to retain title to this invention. Inquiries concerning rights for its commercial use should be addressed to:

*Innovative Technology Assets Management
JPL*

*Mail Stop 202-233
4800 Oak Grove Drive
Pasadena, CA 91109-8099
(818) 354-2240*

E-mail: iaoffice@jpl.nasa.gov

Refer to NPO-30590, volume and number of this NASA Tech Briefs issue, and the page number.

Manufacture of Sparse-Spectrum Optical Microresonators

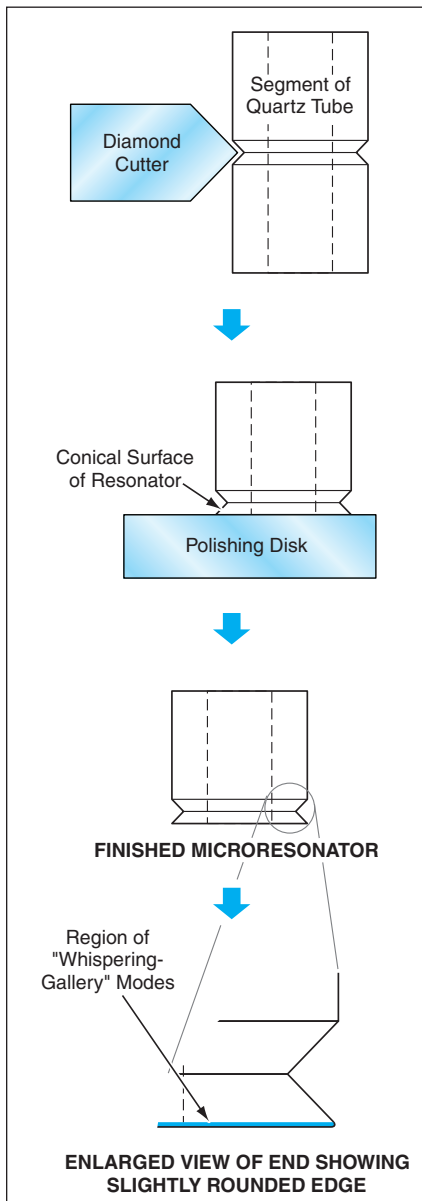
Multiple units having the same spectral parameters could be produced.

NASA's Jet Propulsion Laboratory, Pasadena, California

An alternative design for dielectric optical microresonators and a relatively simple process to fabricate them have been proposed. The proposed microresonators would exploit the same basic

physical phenomena as those of microtorus optical resonators and of the microsphere optical resonators described in several prior *NASA Tech Briefs* articles. The resonances in such devices are asso-

ciated with the propagation of electromagnetic waves along circumferential paths in “whispering-gallery” modes. The main advantage afforded by the proposal is that the design and the fab-



A Microresonator Would Be Fabricated from a length of silica tube by a process of diamond cutting, mechanical polishing, and fire polishing.

rication process are expected to be amenable to production of multiple microresonators having reproducible spectral parameters — including, most notably, high values of the resonance quality factor (Q) and reproducible resonance frequencies.

High- Q optical microresonators are key components in many contemplated advanced optoelectronic applications, including high-stability, narrow-line-width microlasers; spectrometers; remote-sensing systems; memory devices; and optical delay lines. In all such applications, there are requirements for stable and repeatable spectra that contain the resonance spectral lines of interest and do not contain unwanted lines: in other words, there are requirements for microresonators that exhibit high Q with reproducible sparse spectra. Although prior microspheres and microtorus optical resonators have been shown to have the potential to satisfy these requirements, the techniques used heretofore to fabricate them, involving melting individual resonators under manual control, do not yield reproducible spectral parameters and, therefore, are not suitable for production of multiple, functionally identical units.

The figure depicts a microresonator and the fabrication thereof according to the proposal. In preparation for fabrication of a batch of microresonators, one would choose a silica tube of precisely calibrated diameter (typically about 6 mm), so that all the resonators in the batch could be relied upon to have the same diameter. One would cut the tube into shorter segments — one for each resonator. By use of a diamond cutter, a circumferential V

groove would be made on the outer surface of each segment. By polishing with a diamond disk, all the material would be removed from one end of the segment (the lower end in the figure), up to the edge of the groove. Thus, what would remain at the polished end of the tube would be a quasi-toroidal resonator structure having a conical outer surface.

The edge region would be fire-polished by use of a hydrogen/oxygen torch to eliminate the roughness of the cut edge and conical surface and the residual roughness of the mechanically polished end face of the tube segment. This smoothing of the surface would reduce the loss of light propagating in whispering-gallery modes, thereby helping to ensure high Q (anticipated to be 10^9). The fire polishing would also round the edge slightly, but the radius of curvature of the edge would be small enough that the spectrum would remain sparse.

This work was done by Anatoliy Savchenkov, Vladimir Ilchenko, Lute Maleki, and Dimitri Kossakovski of Caltech for NASA's Jet Propulsion Laboratory. Further information is contained in a TSP (see page 1).

In accordance with Public Law 96-517, the contractor has elected to retain title to this invention. Inquiries concerning rights for its commercial use should be addressed to:

*Innovative Technology Assets Management
JPL*

*Mail Stop 202-233
4800 Oak Grove Drive
Pasadena, CA 91109-8099
(818) 354-2240*

E-mail: iaoffice@jpl.nasa.gov

Refer to NPO-30588, volume and number of this NASA Tech Briefs issue, and the page number.

Exact Tuning of High- Q Optical Microresonators by Use of UV

Resonance frequencies can be shifted permanently by controlled amounts.

NASA's Jet Propulsion Laboratory, Pasadena, California

In one of several alternative approaches to the design and fabrication of a "whispering-gallery" optical microresonator of high resonance quality (high Q), the index of refraction of the resonator material and, hence, the resonance frequencies (which depend on the index of refraction) are tailored by use of ultraviolet (UV) light. The principles of operation of optical microres-

onators, and other approaches to the design and fabrication of optical microresonators, have been described in prior *NASA Tech Briefs* articles, including the two immediately preceding this one.

In this approach, a microresonator structure is prepared by forming it from an ultraviolet-sensitive material. Then the structure is subjected to controlled exposure to UV light while its reso-

nance frequencies are monitored. This approach is applicable, for example, to the fabrication of optical microresonators from silica doped with germanium. This material exhibits low optical loss at a wavelength of 1,550 nm — a wavelength often used in optical communication systems. It is also highly sensitive to UV light: its peak sensitivity occurs at a wavelength of 334 nm, and

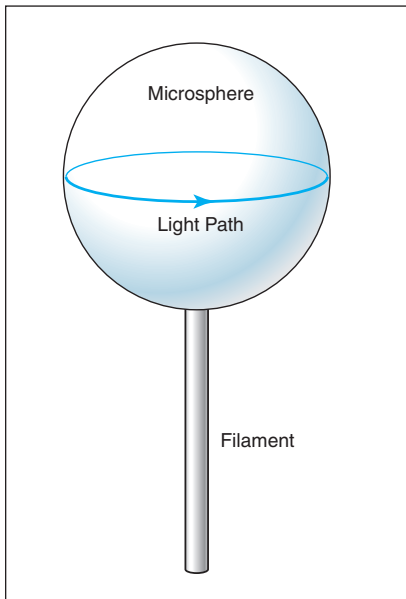


Figure 1. A **Spherical Optical Microresonator** (microsphere) is formed by melting one end of a Ge-doped SiO₂ filament.

its index of refraction can be shifted by as much as 10^{-2} by irradiating it at an argon-ion-laser wavelength of 351 nm.

Fabrication begins with softening a Ge-doped SiO₂ rod by use of a hydrogen/oxygen microburner and stretching the rod into a filament $\approx 30 \mu\text{m}$ wide. The tip of the filament is heated in the hydrogen/oxygen flame to form a sphere having a diameter between about $100 \mu\text{m}$ and about 1 mm (see Figure 1). Then the resonance frequencies of the sphere used as a microresonator are measured while the sphere is irradiated with UV light at a power of 1.5 W from an argon-ion laser that can be operated at either of two wavelengths: 379 or 351 nm. Irradiation at the longer wavelength heats the sphere and thereby temporarily shifts the resonance frequencies but does not cause a permanent change in the index of refraction. Irradiation at

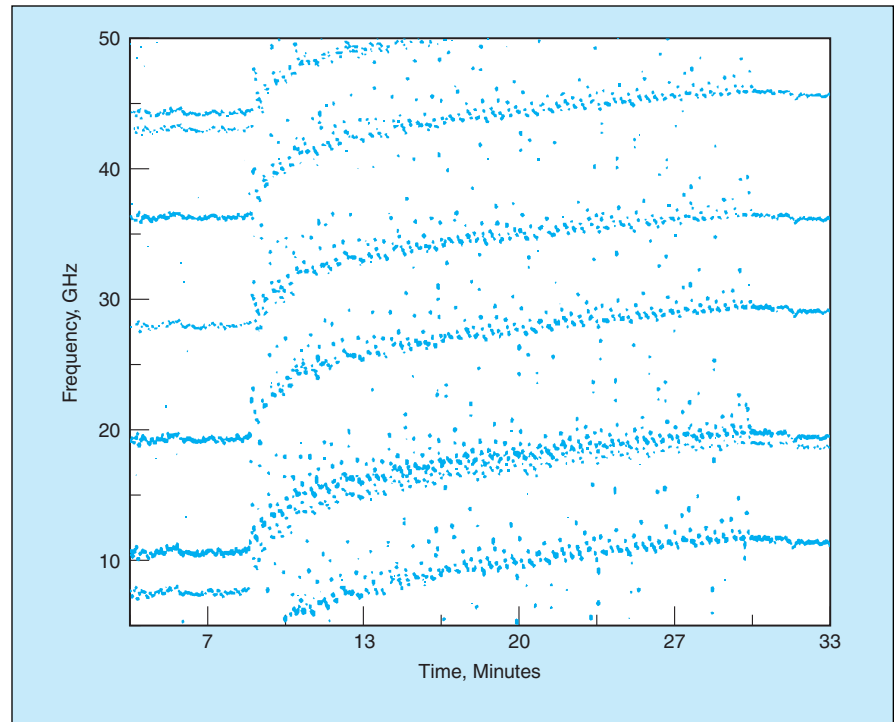


Figure 2. The **Shift in Resonance Frequencies** of a Ge-doped SiO₂ microsphere of 240- μm diameter was measured as a function of time of exposure to laser light at a wavelength of 351 nm.

the shorter wavelength changes the index of refraction permanently.

At first, for the purpose of adjusting the optics that focus the laser light on the sphere, the laser is operated at the longer wavelength and the adjustments performed to maximize the shift of resonance frequencies. Then the laser is operated at the shorter wavelength while the resonance frequencies are monitored. The UV radiation is terminated when the resonance frequencies have shifted by the desired amount. For example, a typical shift of ≈ 10 GHz can be achieved in a microsphere of 240- μm diameter (see Figure 2).

This work was done by Anatoliy Savchenkov, Lute Maleki, Vladimir

Ilchenko, and Timothy Handley of Caltech for NASA's Jet Propulsion Laboratory. Further information is contained in a TSP (see page 1).

In accordance with Public Law 96-517, the contractor has elected to retain title to this invention. Inquiries concerning rights for its commercial use should be addressed to:

*Innovative Technology Assets Management
JPL*

*Mail Stop 202-233
4800 Oak Grove Drive
Pasadena, CA 91109-8099
(818) 354-2240*

E-mail: iaoffice@jpl.nasa.gov

Refer to NPO-30589, volume and number of this NASA Tech Briefs issue, and the page number.



Automation for “Direct-to” Clearances in Air-Traffic Control

Air-traffic controllers can be more productive and flight times can be reduced.

Ames Research Center, Moffett Field, California

A method of automation, and a system of computer hardware and software to implement the method, have been invented to assist en-route air-traffic controllers in the issuance of clearances to fly directly to specified waypoints or navigation fixes along straight paths that deviate from previously filed flight plans. Such clearances, called “direct-to” clearances, have been in use since before the invention of this method and system. Usually, they are issued when requested by pilots; less frequently, controllers issue them on their own initiatives.

A typical flight-plan trajectory consists of multiple straight segments. As such, it cannot minimize flight time because it deviates from both a great circle and from the shortest-flight-time non-great-circle trajectory that could theoretically be generated if the wind field at every point in space and time could be predicted and taken into account in assessing alternative trajectories. Given these complications, it is sometimes possible to save time by flying along an alternative straight-line segment that bypasses a flight-plan waypoint: this is the main reason for seeking and issuing a direct-to clearance.

The primary requirement guiding the design of the present system was to increase the productivity of controllers and the efficiency of aircraft trajectories within the constraints of the current air-traffic-control environment. This requirement ruled out dependence on such new infrastructure as automated two-way air/ground data links. It also eliminated from consideration the specification of curved or multi-segment trajectories that provide the minimum time to fly to destinations in spatially varying wind fields: neither the infrastructure of today’s air-traffic control system nor the navigation equipment on most aircraft support the specification of such types of trajectories to aircraft while in flight.

The system utilizes four-dimensional (time plus three spatial coordinates) trajectory information generated by the Center-TRACON (terminal radar approach control) Automation System (CTAS), which is in current use by air-traffic

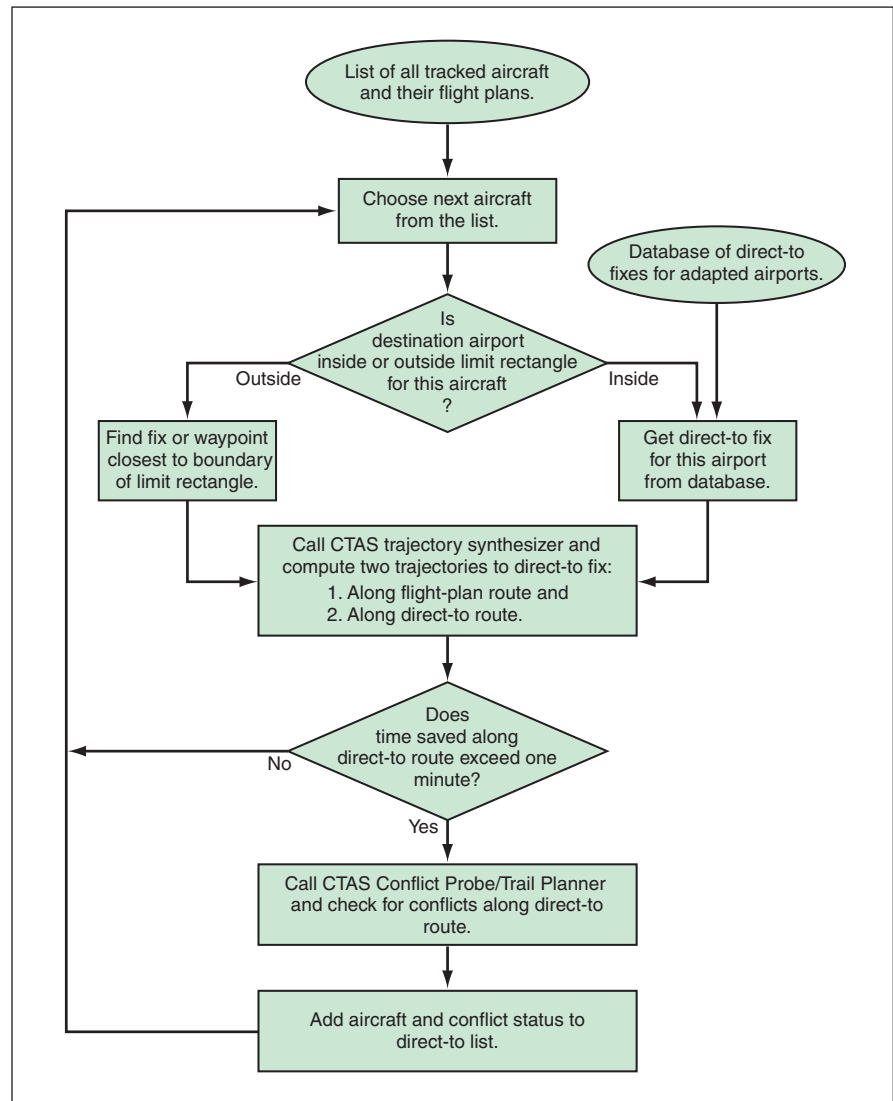


Figure 1. The Flowchart illustrates the steps of computation and decision in the automated generation of a list of aircraft eligible for direct-to clearances.

control. The CTAS trajectory computations utilize all known information about an aircraft, including its capabilities, its current three-dimensional coordinates and velocity, and meteorological conditions (including winds) specified on a grid that spans the entire airspace of the continental United States.

The system first finds all aircraft flying on inefficient routes, then determines whether it is possible to save time by by-

passing some route segments, whether potential direct-to fixes lie within a rectangular geographical area that contains the air-traffic-control center using the system, then finally determines whether the improved route is free of conflicts with other aircraft (see Figure 1). Aircraft that survive these tests are considered to be eligible for direct-to clearances. The system displays a list of all eligible aircraft in order of decreasing



Figure 2. This Display helps the controller identify and work with the highest-pay-off aircraft.

potential time savings. This list enables an air-traffic controller (see Figure 2) to easily identify and work with the highest-pay-off aircraft, thereby contributing to a significant increase in the productivity of both the air-traffic controller and the aircraft. Another display generated by the system is a graphical user interface, through which the air-traffic controller can issue the direct-to clearance to the aircraft by a simple point-and-click action on a computer mouse.

This work was done by Heinz Erzberger and David McNally of Ames Research Center. Further information is contained in a TSP (see page 1).

This invention has been patented by NASA (U.S. Patent No. 6,314,362). Inquiries concerning rights for the commercial use of this invention should be addressed to the Ames Technology Partnerships Division at (650) 604-2954. Refer to ARC-14359-1.



Improved Traps for Removing Gases From Coolant Liquids

Two documents discuss improvements in traps for removing noncondensable gases (e.g., air) from heat-transfer liquids (e.g., water) in spacecraft cooling systems. Noncondensable gases must be removed because they can interfere with operation. A typical trap includes a cylindrical hydrophobic membrane inside a cylindrical hydrophilic membrane, all surrounded by an outer cylindrical impermeable shell. The input mixture of gas bubbles and liquid flows into the annular volume between the membranes. Bubbles pass into the central hollow of the hydrophobic membrane and are vented. The liquid flows outward through the hydrophilic membrane and is recirculated. The proposed improvements include the following:

1. The outer membrane would be made of a more hydrophilic, commercially available material so that membrane pores could be made smaller without increasing the pressure drop. Decreasing the pore size would increase the bubble pres-

sure, thereby increasing the degree of retention of bubbles in the trap.

2. Multiple hydrophobic membranes would be used to increase venting area at the downstream end, where bubbles tend to collect.
3. Upstream of the venting area, the hydrophobic membranes would be coated with a dense polymer to reduce evaporation of the coolant liquid.

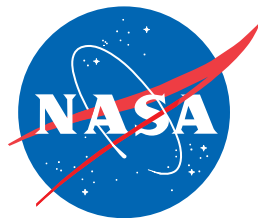
This work was done by John Holladay of Marshall Space Flight Center and Stephen Ritchie of the University of Alabama. For further information, contact Sammy Nabors, MSFC Commercialization Assistance Lead, at sammy.a.nabors@nasa.gov. MFS-32037-1

Lunar Constellation of Frozen Elliptical Inclined Orbits

A document discusses the design of orbits of spacecraft for relaying communications between Earth stations and robotic and human explorers in craters in one of the polar regions on the Moon. In simplest terms, the basic problem is to design a constellation of orbits to provide continuous and preferably re-

dundant communication coverage of one of the poles with a minimal number of spacecraft and little or no controlled maneuvering of the spacecraft to maintain the orbits. The design method involves the use of analytical techniques for initial selection of orbits, followed by a numerical procedure for tuning the coverage of the constellation to obtain a design. In an example application, the method leads to a constellation of three spacecraft having elliptical, inclined orbits, the apoapsides of which would remain in the hemisphere (North or South) containing the pole of interest. The orbits would be stable and would maintain the required spacecraft formation for at least 10 years, without need for controlled maneuvering if gravitation is the only force considered to affect the orbits. A small amount of controlled maneuvering would be needed to counteract effects of solar-radiation pressure and other perturbations.

This work was done by Todd Ely and Gary Noreen of Caltech for NASA's Jet Propulsion Laboratory. Further information is contained in a TSP (see page 1). NPO-40992



National Aeronautics and
Space Administration